Case Studies in Thermal Engineering 64 (2024) 105448

Contents lists available at ScienceDirect

Case Studies in Thermal Engineering

journal homepage: www.elsevier.com/locate/csite

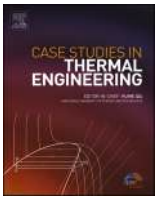

# The performance analysis of a compressed air energy storage (CAES) for peak moving with cooling, heating, and power production

Ehsanolah Assareh [a,b,c], Siamak Hoseinzadeh [d], Abolfazl Karami [a], Hassan Bazazzadeh [e,*], Daniele Groppi [f], Davide Astiaso Garcia [d]

[a] Department of Renewable Energy Technology, Materials and Energy Research Center, Dezful Branch, Islamic Azad University, Dezful, Iran
[b] Department of Mechanical Engineering, Faculty of Advanced Technologies, Quchan University of Technology, Quchan, Iran
[c] Built Environment and Engineering Program, College of Sport, Health and Engineering (CoSHE), Victoria University, Melbourne, Australia
[d] Department of Planning, Design, and Technology of Architecture Sapienza University of Rome, Rome, 00196, Italy
[e] Urban Energy Systems Lab, Swiss Federal Laboratories of Material Science and Technology (Empa), Ueberlandstrasse 129, 8600, Düebendorf, Switzerland
[f] Dipartimento di Scienze Umane e Sociali, Patrimonio Culturale, CNR - Consiglio Nazionale Delle Ricerche, USA

ARTICLE INFO

Handling Editor: Dr Y Su

*Keywords:*
Geothermal energy
Multi energy production system
Compressed air energy

ABSTRACT

This study focuses on modeling and optimizing a multifaceted geothermal-based energy production system within the context of Denmark. The primary objectives revolve around enhancing system efficiency and reducing operational costs. The system under investigation comprises geothermal components, an organic Rankine cycle, a compressed air energy storage facility, and an absorption chiller. The organic Rankine cycle operates using refrigerants R123 and ammonia, effectively converting thermal energy into electricity and thermal energy for various applications. Optimization was carried out employing the Response Surface Method in tandem with Design-Expert software, facilitating the fine-tuning of objective functions. Two key objectives were selected: Exergy Round Trip Efficiency and cost rate, aimed at improving technical performance and curbing economic expenditure. A range of design variables were considered for optimization, including turbine and pump inlet temperatures, geothermal mass flow rate, turbine and pump efficiencies, compressor and gas turbine efficiency, inlet pressure to the compressed air energy storage tank, and evaporator pinch point temperature. The system reached an impressive exergy efficiency peak of 77.98 %, accompanied by a modest cost rate of 5.48 $/h. The costliest components in the system were the compressed air energy storage unit, followed closely by organic Rankine cycle 1 and organic Rankine cycle 2. In contemplating the practical implementation of this innovative energy system, ten cities in Denmark underwent rigorous analysis, accounting for technical and economic factors. Subsequent assessments identified Aarhus as the optimal location to initiate the system. The environmental results showed that by producing 13981.9 MW of electricity annually in Arhus City, it is possible to help reduce $CO_2$ emissions by 2853.2 tons of $CO_2$/year and avoid environmental costs of 68455.3 $/year. The environmental assessment also highlighted the potential for substantial green space expansion, estimating an additional 13 ha of green areas in the city of Aarhus, Denmark.

* Corresponding author.
*E-mail addresses:* siamak.hosseinzadeh@unirmoa1.it, hoseinzadeh.siamak@gmail.com (S. Hoseinzadeh), hassan.bazazzadeh@empa.ch (H. Bazazzadeh).

https://doi.org/10.1016/j.csite.2024.105448
Received 14 April 2024; Received in revised form 3 September 2024; Accepted 5 November 2024
Available online 6 November 2024

Nomenclature

| | | | |
|---|---|---|---|
| $C_P$ | Specific heat of air and water at constant pressure [kJ/kg.K] | cv | control volume |
| E | Energy | DOE | design of experiments |
| $\dot{E}x$ | *Exergy [kW]* | e | out |
| $EX_D$ | Exergy destruction [kW] | EES | Engineering Equations Solver |
| g | Gravitational acceleration | ERTE | Exergy round trip efficiency [%] |
| *h* | *Specific enthalpy [kj/kg]* | eva | Evaporator |
| m | *Mass flow [kg/s]* | HEX | heat exchanger |
| $\dot{m}$ | *Mass flow rate [kg/s]* | i | in |
| P | Pressure [kPa] | *n* | *Number* |
| $\dot{Q}$ | *Heat transfer rate [kW]* | ORC | Organic Rankine Cycle |
| s | Specific entropy [kJ/kg.K] | ph | physical |
| T | Temperature [°C] | RSM | response surface methodology |
| t | Time [h] | tur | Turbine |
| U | Overall heat transfer coefficient [kW/m$^2$K] | 0 | Dead state |
| *W* | *Power [kW]* | Greek symbol | |
| x | Salinity [ppm] | $\eta$ | *efficiency* |
| Z | Height | $\varphi$ | *Maintenance factor* |
| Subscripts | | | |
| ch | Chemical | | |
| Comp | Compressor | | |
| cond | Condenser | | |

## 1. Introduction

In the modern era, energy consumption stands as a linchpin for both industrial processes and power generation, while its relevance extends to the very core of residential life [1]. Yet, an overwhelming reliance on fossil fuels to satiate this hunger for energy has brought about a slew of disconcerting issues, casting a long, looming shadow over our global ecosystem. The substantial drawbacks of fossil fuel consumption include a glaring contribution to environmental pollution, the exacerbation of greenhouse gases, which, in turn, fuels the relentless engine of global warming. As the mercury climbs and polar ice caps recede, the very contours of our planet undergo dramatic and irreversible transformations. Moreover, the production, transportation, and consumption of fossil fuels are plagued by staggering costs and an intricate web of logistical challenges, further underscoring the imperativeness of an alternative energy paradigm. Exploring the myriad concomitant challenges in the pursuit of fossil fuels, it becomes increasingly evident that the transition to renewable energy sources is not merely a matter of choice but an imperative, necessitated by the pressing need to address the multifaceted concerns arising from fossil fuel dependency. Unlike their finite, non-renewable counterparts, renewable energy sources offer the invaluable virtue of cyclicality, allowing energy to return to nature in a sustainable loop [2]. Among these sustainable energy sources, geothermal energy emerges as a veritable titan in the realm of clean energy solutions, offering a unique opportunity to reduce the carbon footprint that looms as an existential threat. The deployment of geothermal energy not only mitigates the immediate concerns surrounding environmental degradation but also positions itself as a staunch guardian against the ravaging impacts of climate change [3,4]. However, the efficient utilization of renewable energies, including geothermal, necessitates an adept solution for the intermittent nature of these energy sources, propelling the need for innovative energy storage systems [5]. In the realm of energy storage, the compressed air energy storage system takes center stage as a prominent solution, receiving considerable attention for its remarkable capacity to store energy effectively, thereby bolstering overall system efficiency [6]. Its versatile and adaptable nature aligns well with the intermittent energy flows from renewable resources, effectively bridging the gap between energy generation and consumption. With this backdrop, it becomes increasingly apparent that the collective pursuit of renewable energy sources, particularly in the context of geothermal energy, and their seamless integration with advanced energy storage solutions holds the promise of an energy landscape that not only fulfills our immediate energy requirements but also safeguards the world against the detrimental impacts of fossil fuel dependency. This convergence of innovative technologies and a sustainable energy ethos usher in a paradigm shift, one where the energy we derive today doesn't compromise the energy needs of the future. A comprehensive examination of recent studies reveals an active and evolving landscape within the realm of renewable energy. Researchers are diligently exploring innovative ways to harness cleaner energy sources while optimizing energy systems and addressing environmental challenges. The following summarization highlights the significant findings and overarching themes across these studies:

Razmi et al. (2021): Razmi and colleagues delved into the realm of Compressed Air Energy Storage (CAES) systems, investigating wind speed fluctuations in the Abhar and Kahek sites. Their results illuminated the potential for CAES facilities to inject substantial power into the grid during peak demand periods in July, August, and September, with notable round-trip efficiencies [7]. Razmi et al. (2019): In a bid to foster environmental sustainability, Razmi et al. ventured into the development of a multi-production system. This integrated system employed an Organic Rankine Cycle (ORC), CAES system, and absorption refrigeration cycle to concurrently produce electrical energy and cooling capacity, yielding noteworthy outcomes [8]. Razmi and Janbaz (2020): Razmi and Janbaz explored the realms of exergy and economic evaluations within the context of a clean cogeneration system. Their research pinpointed cost increments in electricity and cold water during peak consumption periods, underscoring the importance of reliability [9]. Alirahmi et al. (2021): In 2021, Alirahmi and team explored a distinctive synergy between a compressed air energy storage system and solar and desalination units. This unique system harnessed solar energy to elevate the air turbine's inlet temperature, a novel approach contributing to environmental compatibility [10]. Alirahmi et al. (2021): Alirahmi et al. ventured into the domain of solid oxide fuel cells, concomitant with compressed air energy storage. They succeeded in optimizing the ERTE, total cost rate, and $CO_2$ emissions to

commendable values at the system's optimal point [11]. Seiiedhoseiny et al. (2022): Seiiedhoseiny and colleagues delved into the domain of geothermal energy, scrutinizing a multi-generation system. By manipulating the flash tank pressure, they managed to augment cooling and heating loads significantly, albeit with a reduction in net power generation [12]. Pan et al. (2023): In the same year, Pan and co-researchers probed integrated systems for power generation. They scrutinized various configurations exploiting the cold energy of liquefied natural gas and geothermal energy, identifying strategies to enhance energy efficiency and exergy [13]. Jiansheng et al. (2022): In 2022, Jiansheng et al. embarked on a numerical exploration of advanced geothermal systems equipped with horizontal wells. Their findings unveiled a rapid decrease in geothermal fluid outlet temperature with increased mass flow rates, emphasizing the pivotal role of mass flow in system performance [14]. Li et al. (2020): Li and his team examined a multi-energy production system characterized by a symbiotic union of a geothermal heat pump, solid oxide fuel cell, and biomass fuel. Their system employed hot exhaust gases from biomass fuel to generate electrical energy, achieving commendable energy and exergy efficiencies [15]. Al-Hamed and Dincer (2019): Al-Hamed and Dincer probed a hybrid system that harnessed solar and geothermal energy via an ejector-absorption hybrid cycle. Their research illuminated the sensitivity of system energy efficiency to ambient temperature variations and underscored the potential for efficiency enhancements through ejector optimization [16]. Briolaa et al. (2019): In 2019, Briolaa and collaborators explored a hybrid geothermal power plant uniquely designed to produce clean electrical energy via an Organic Rankine Cycle (ORC) fed by a biomass heat source through an intermediate geothermal fluid [17]. Zhong et al. (2023): In the same year, Zhong et al. undertook a feasibility study of clean electricity production through advanced geothermal systems employing vertical wells. Their research was based on geological data and offered insights into the potential of clean electricity generation from geothermal sources [18]. Mardan Dezfouli et al. (2023): Mardan Dezfouli and co-researchers ventured into the domain of geothermal-based electricity generation. They introduced and optimized a unique three-geothermal-cycle system to bolster electricity production while keeping exergy destruction in check [19]. Ghorbani et al. (2020): In 2020, Ghorbani et al. pioneered a multi-energy production system with a dual mission of electricity generation and fresh water production using renewable energies. Their innovation channeled heat from the system's condenser for efficient desalination, making a significant contribution to freshwater production [20]. Karapekmez and Dincer (2020): In a 2020 study, Karapekmez and Dincer embarked on a comparison of the efficiency and environmental impact of a combined cycle leveraging solar energy and diverse fuel cell technologies. Their findings spotlighted the viability of alternative fuels, particularly wood and sawdust, for reduced $CO_2$ emissions [21]. Montazerinejad et al. (2019): In 2019, Montazerinejad and their team scrutinized a multi-energy production system hinging on solar renewable energy. Their work uncovered the thermal energy storage tank as a focal point for exergy destruction in the system [22].

According to the surveys, a lot of research has been done on the use of renewable energy for energy production. In the studies conducted, more on the use of renewable energy, especially solar and wind energy have been used to produce different energies. In the reviewed studies, the use of geothermal energy to start renewable systems has received less attention. According to studies, the use of compressed air energy storage units to increase the production capacity of the system and help supply residential, office, and commercial buildings with electricity during peak consumption time has been given less attention. Researchers have done extensive research on the use of batteries to store energy and increase the stability of renewable systems, but due to the high cost and high maintenance of batteries, researchers are thinking of replacing batteries. Using the air compression method is a new technology for electric power storage that needs more studies. In the proposed system, excess electricity can be used for air compression. To use the electricity stored by the CAES method, it is enough to direct the compressed air to a gas turbine to generate electricity. In theory, this method is efficient and practical; Because it can be used at a very low cost, and it is the cheapest way to store energy. On the other hand, using this method compared to other methods does not require any special geographical conditions. Collectively, these studies underscore the constant quest for innovative, environmentally responsible energy solutions and the critical role of exergy, efficiency, and multi-generation approaches in shaping the future of sustainable energy production and utilization.

The research we've described is a comprehensive study focusing on the development and optimization of a geothermal-based renewable energy system for electricity, heating, and cooling production. The main objectives and activities of the research can be summarized as follows.

1. **System Introduction:** The research aims to introduce a novel energy system that combines geothermal well units, two Organic Rankine Cycle (ORC) units, and a single-effect absorption chiller. This integrated system is designed for maximum power generation, cooling, and heating while minimizing harmful environmental effects.
2. **Energy, Exergy, and Economic Analyses:** The research includes energy and exergy analyses, which assess the energy efficiency and resource utilization of the proposed system. Additionally, economic analyses are conducted to determine the cost-effectiveness of the system.
3. **Multi-Objective Optimization:** Multi-objective optimization is performed using the response surface method. The objective functions considered for optimization are likely related to system performance, such as exergy efficiency and cost rate, to achieve the best possible trade-offs between technical and economic parameters.
4. **Economic Analysis:** The study investigates the economic aspects of the proposed system by determining the costs associated with individual units and components, enabling a detailed assessment of the economic feasibility of the project.
5. **Feasibility and Reliability:** The research evaluates the feasibility and reliability of the geothermal system by considering various weather data from different regions in Denmark. This analysis helps identify the best-suited location for implementing the system based on climatic conditions.
6. **Environmental Analysis:** The environmental analysis assesses the potential environmental benefits of the proposed geothermal system. This may include estimates of carbon emissions reductions, reduced pollution, and other positive environmental impacts.

In summary, the research aims to develop an innovative geothermal energy system that harnesses the Earth's natural heat to produce electricity, heating, and cooling, with a strong focus on sustainability, economic viability, and environmental friendliness. By combining technical analyses, economic evaluations, and environmental assessments, the study seeks to provide a holistic understanding of the proposed system's potential benefits and to determine the most suitable location for its implementation in Denmark. In this research, by using geothermal renewable energy in a new renewable system with climatic conditions and close to areas with high potential for this system and with suitable conditions, clean electricity, heating, and cooling energy have been produced. The purpose of this research is to reduce environmental pollution and produce products that are produced without interference from fossil energy and are vital energies of society's life. Also, in this research, the performance of the system is examined in the weather conditions of different regions in Denmark, and the most suitable regional location for the construction of the proposed power plant is determined.

## 2. System description

Fig. 1 provides an overview of the proposed geothermal energy system, including its main components and the flow of energy and materials within the system. Here is an explanation of the key components and processes.

1. **Geothermal Wells Sub-System:** The geothermal energy system begins with the geothermal wells that tap into the Earth's geothermal reservoirs. These wells access the natural heat stored in the Earth's crust.
2. **ORC (Organic Rankine Cycle) with Organic Refrigerant and Ammonia:** The heart of the system is the ORC, which operates using an organic refrigerant fluid (possibly in combination with ammonia). The ORC system plays a central role in converting the geothermal heat into electricity. It uses the heat from the geothermal reservoir to generate power, which can then be used for various purposes.

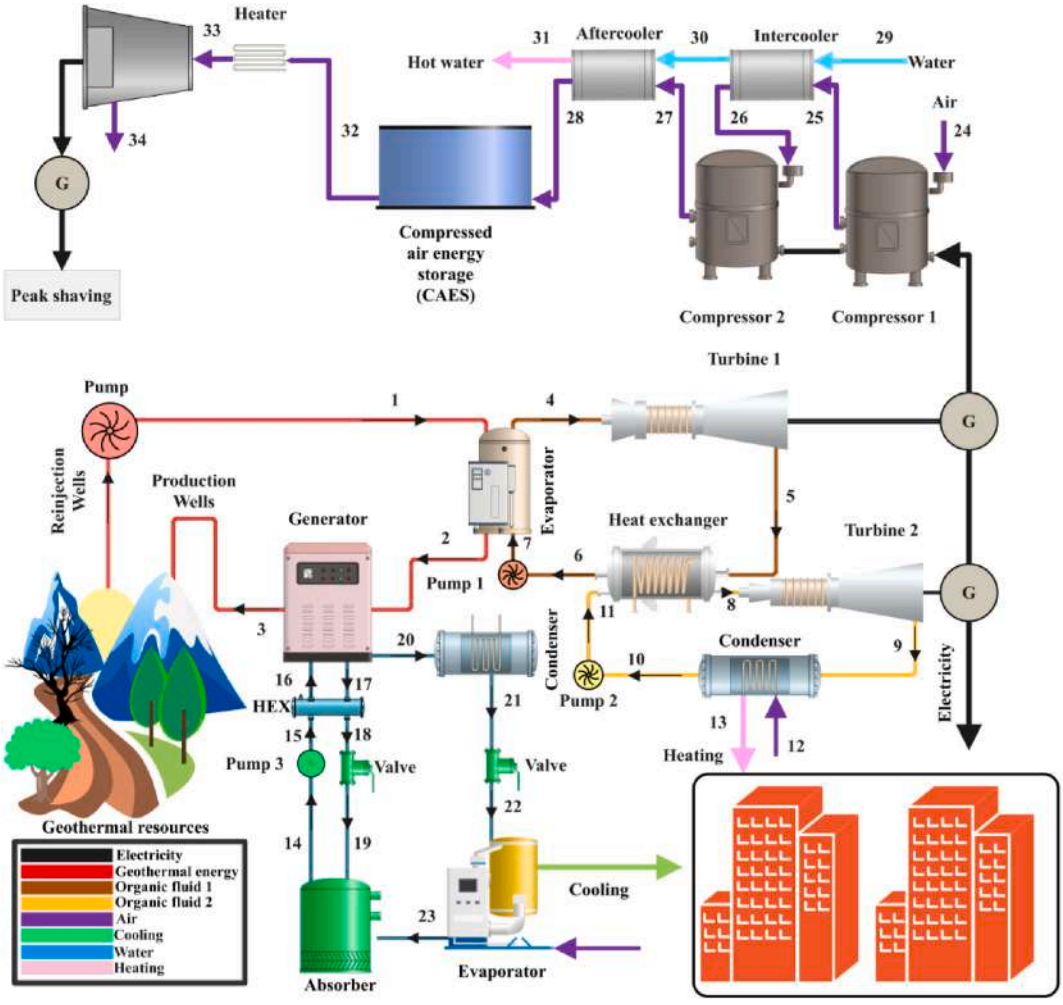


**Fig. 1.** Schematic of the system.

3. **Absorption Chiller:** This component is responsible for producing cooling. It uses heat generated in the system to drive the cooling process, which can be used for air conditioning or cooling applications.
4. **Energy Storage System with Compressed Air:** The system includes an energy storage system that utilizes compressed air. Energy can be stored when excess power is available, and this stored energy can be released when needed, helping to balance the electrical grid and ensure a continuous power supply.
5. **Clean Electricity, Cooling, and Heating Production:** The system's primary products are clean electricity, cooling (produced by the absorption chiller), and heating (which can be a byproduct of the overall process). These outputs can be used to meet the energy needs of various applications, including residential, commercial, and industrial sectors.

The system leverages low-temperature geothermal heat sources to drive the ORC turbine, which, in turn, generates electricity. The geothermal fluid, which is used as the heat source, flows through the evaporator to provide heat to the ORC cycle. After this step, the fluid is re-injected into the ground for a sustainable heat source.

Pumps play a role in moving the geothermal fluid from the reservoir to the evaporator and ensuring a continuous flow. Additionally, the system may include other equipment like turbines and compressors to facilitate energy conversion and storage.

Overall, the geothermal energy system described in Fig. 1 demonstrates a comprehensive approach to utilizing geothermal resources for clean energy production and heating and cooling applications, contributing to sustainable and environmentally friendly energy solutions.

Since its inlet and outlet fluid pressure is constant, there is no need to change the fluid phase, and it also has a low power consumption, which can be ignored in calculations. The input geothermal heat causes the evaporation of the fluid in the evaporator and through the evaporator heats the Raniken cycle turbine (point 4). Then, through point 2, it enters the refrigeration cycle generator to produce cooling, and at the last stage, through point 3, it is re-injected into the ground. The temperature of the fluid injected from the geothermal well to the organic cycle evaporator is 210 °C and its flow rate was considered 1.5 kg/s. In Rankine's organic cycle, power is produced by turbines, and at points 5 and 9, the heat output from the turbines enters the condensers for the cooling process. Then, at points 6 and 10, the fluid coming out of the condensers enters the pumps and the cycle process continues in the same way. During the process of the system, the electricity of the system drives the compressor to compress the ambient air. Compressed air is then stored in the CAES source for later use during periods of peak demand. To minimize the power consumption in the compressors and to recover the waste heat generated in the compression process for the desalination unit, two coolers are applied between the compressors. Therefore, the ambient air absorbs the heat released in the intercoolers and reduces the volume of the storage tank by reducing the temperature of the air coming out of the last compressor in the aftercooler.

## 3. System analysis

In the thermodynamic analysis of the geothermal system, several assumptions and basic relationships were used to simplify the problem and perform the necessary calculations. These include.

1. **Steady-State Conditions:** The system operates under steady-state conditions, meaning that it doesn't change with time.
2. **Isentropic Turbines and Pumps:** Turbines and pumps are assumed to be isentropic, which means they operate with maximum efficiency.
3. **Insignificant Pressure Drops in Pipelines:** Pressure drops in the pipelines are considered insignificant.
4. **Saturated Output in Condenser and Evaporator:** The output of the condenser is assumed to be saturated liquid, and the output of the evaporator is assumed to be saturated steam.
5. **Insignificant Changes in Kinetic Energies:** Changes in kinetic energies of the fluids are considered negligible.
6. **Insignificant Changes in Potential Energies:** Changes in potential energies of the fluids (due to changes in elevation) are also considered negligible.

**Table 1**
Amount of input data.

| Parameter | Value |
|---|---|
| $\dot{m}_1$ | **1.5 kg/s** |
| $T_1$ | **210°C** |
| $T_4$ | **150°C** |
| $T_6$ | **70°C** |
| $\eta_{turbin}$ | **0.85** |
| $\eta_{pump}$ | **0.8** |
| $pp_{Eva}$ | **5°C** |
| $T_8$ | **60°C** |
| $\eta_{Compressor}$ | **0.86** |
| $\eta_{turbin.Gas}$ | **0.86** |
| $\eta_{Intercooler}$ | **0.85** |
| $\eta_{Aftercooler}$ | **0.85** |
| $P_{28}$ | **5000 kPa** |

The thermodynamic analysis involves applying the laws of conservation of mass and conservation of energy, as well as the principles of energy balance and exergy (a measure of the available work in a system). Additionally, economic analysis, including the cost rate relationship, is used to evaluate the system from a financial perspective. Table 1 provides the input data needed for the geothermal system analysis, which serves as the basis for conducting the thermodynamic and economic assessments of the system's performance. These data points are crucial for understanding and modeling the behavior of the system and determining its efficiency and economic feasibility. The thermodynamic analysis is a fundamental step in evaluating the performance of the geothermal system, ensuring that it operates as efficiently as possible while adhering to the given assumptions and constraints [23,24].

The production capacity of the double ORC:

$$\dot{W}_{net} = \dot{W}_{net,ORC\ 1} + \dot{W}_{net,ORC\ 2} \tag{1}$$

The amount of production power of the entire system at peak time is obtained from Eq. (2):

$$\dot{W}_{net\ peak\ shaving} = \dot{W}_{net} + \dot{W}_{GT} - \dot{W}_{CAES} \tag{2}$$

The cost rate of the whole system is obtained from the total cost of the system components, and is calculated according to Equation (3):

$$Z_{total} = Z_{Turbine1} + Z_{Turbine2} + Z_{cond} + Z_{evap} + Z_{Pump1} + Z_{Pump2} + Z_{Chiller} + Z_{HEX} + Z_{Comp\ 1} + Z_{Comp\ 2} + Z_{CAES\_tank} + Z_{Aftercooler} + Z_{Intercooler} + Z_{Turbin\ Gas} \tag{3}$$

Exergy round trip efficiency (ERTE) relationship [25]:

$$ERTE = \left(\dot{W}_{net} \times 24 + Q_{cooling} \times 24 + \dot{W}_{GT} \times T_{discharge}\right) \times 100 \,/\, \left(\dot{E}x_1 \times 24 + \dot{W}_{Input\_CAES} \times T_{charge} + Q_{heater} \times T_{discharge}\right) \tag{4}$$

### 3.1. Response level method

The Response Surface Method (RSM) is a powerful set of statistical and mathematical techniques used for constructing empirical models and optimizing processes when multiple independent variables affect a response or output. The primary aim of response surface designs is to determine the optimal conditions for a process or system by exploring how changes in the independent variables impact the response.

Fig. 2 outlines the solution process using the Response Surface Method and can be summarized in the following steps.

1. **Identify the Independent Variables:** Start by identifying the independent variables or factors that you want to investigate. These factors are the variables you believe influence the response or output of interest.
2. **Design a Set of Experiments:** Plan and conduct a series of experiments, also known as runs, to collect data on how variations in the independent variables affect the response. The choice of experiments should be designed to gather the most information with the fewest number of runs. Common experimental designs include full factorial, fractional factorial, and central composite designs.

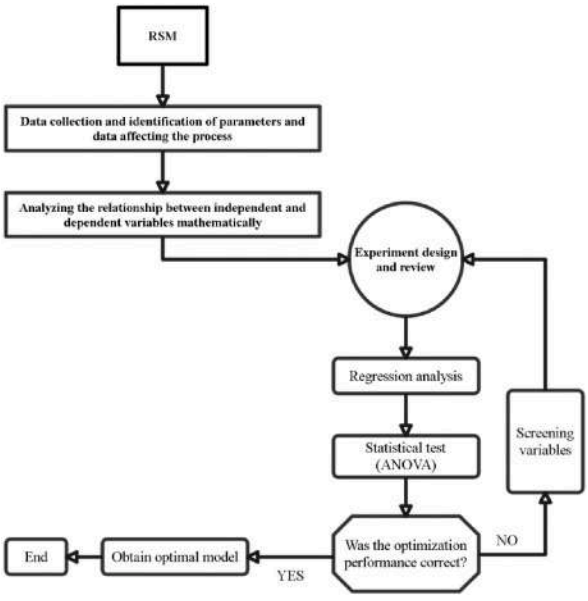


**Fig. 2.** Flowchart of response surface method solution.

3. **Perform the Experiments:** Execute the experiments according to the planned design. Record the responses for each experiment, ensuring that the data is collected accurately and consistently.
4. **Construct Empirical Models:** Use the collected data to build empirical models that describe the relationship between the independent variables and the response. These models are typically polynomial equations or mathematical functions that provide insight into the system's behavior.
5. **Optimize the Response:** Employ the empirical models to identify optimal conditions for the process or system. Optimization involves finding the combination of independent variable settings that results in the desired response, whether that is maximizing, minimizing, or achieving a target value.
6. **Perform Validation Runs:** Conduct a set of validation runs using the optimized conditions to verify that the predictions from the empirical models hold in practice.
7. **Analyze and Interpret Results:** Evaluate the results, considering the trade-offs and implications of the optimal conditions, and make informed decisions based on the analysis.

The Response Surface Method is a valuable tool for designing experiments, exploring complex systems, and optimizing processes efficiently. It allows you to gain insights into the relationships between variables and make data-driven decisions to achieve the best outcomes [26,27].

### *3.2. Topsis method*

The Technique for Order of Preference by Similarity to Ideal Solution (TOPSIS) is a multi-criteria decision-making method used to evaluate and prioritize options based on predefined criteria. The key idea in TOPSIS is to measure the similarity of each alternative to an ideal solution while considering the distance from an ideal point and a negative ideal point.

Fig. 3 represents the flowchart of the TOPSIS method, which includes the following steps.

1. **Identify Decision Alternatives:** List the available decision alternatives (e.g., different locations, configurations, or scenarios) that you want to evaluate.

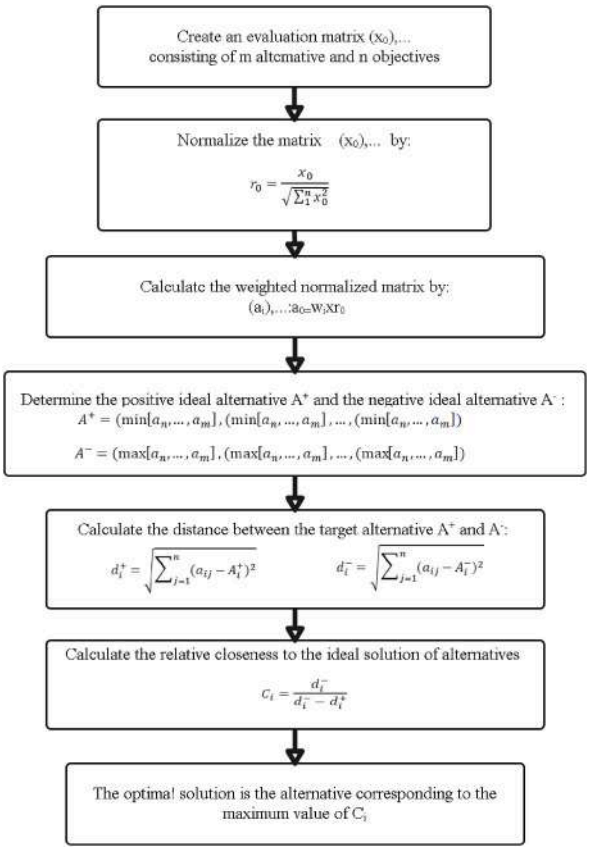


**Fig. 3.** Topsis method.

2. **Establish Evaluation Criteria:** Define the criteria and factors that are relevant to your decision. These criteria can be quantitative or qualitative, and they represent the aspects you want to consider when making your decision.
3. **Normalize the Decision Matrix:** In this step, the decision matrix, which contains data for each alternative with respect to each criterion, is normalized. This normalization ensures that criteria with different units and scales are treated consistently. Common normalization methods include min-max normalization and vector normalization.
4. **Determine the Weight of Criteria:** Assign weights to each criterion to express their relative importance in the decision-making process. These weights are typically based on your preferences and the significance of each criterion.
5. **Calculate the Normalized Weighted Decision Matrix:** Multiply the normalized decision matrix by the weights of criteria. This step emphasizes the importance of each criterion for each alternative.
6. **Identify the Positive Ideal Solution and Negative Ideal Solution:** Determine the ideal solution (the best values for each criterion) and the negative ideal solution (the worst values for each criterion).
7. **Calculate the Separation Measures:** Compute the distance between each alternative and the ideal and negative ideal solutions. These measures indicate how well each alternative performs with respect to the ideal and negative ideal points.
8. **Calculate the Relative Closeness to the Ideal Solution:** Evaluate the relative proximity of each alternative to the ideal solution by considering both its similarity to the ideal solution and its dissimilarity to the negative ideal solution.
9. **Rank Alternatives:** Sort the alternatives based on their relative closeness to the ideal solution. The alternative with the highest relative closeness is considered the most preferred.

TOPSIS is a valuable tool for complex decision-making processes where multiple criteria need to be considered. It helps in objectively selecting the best alternative based on a combination of criteria, weights, and their relative performance [28,29].

### 3.3. Research methodology

The methodology flowchart for this research is outlined in Fig. 4. The overall process can be summarized as follows.

1. System modeling is conducted using engineering equation-solving software.
2. Multi-objective optimization is performed to identify the optimal technical and economic operating conditions of the system.
3. Optimization is executed through Design-Expert software and the response surface method, involving two objective functions: exergy efficiency and cost rate.
4. An economic analysis is carried out to assess the performance of different units and components within the system.
5. Ten cities across Denmark are chosen, each representing different climates and weather conditions, to evaluate the system's performance.
6. Weather data for these various cities is collected using Metanorm software.
7. The best location in Denmark is selected for the system deployment.
8. An environmental analysis is conducted for the chosen city.

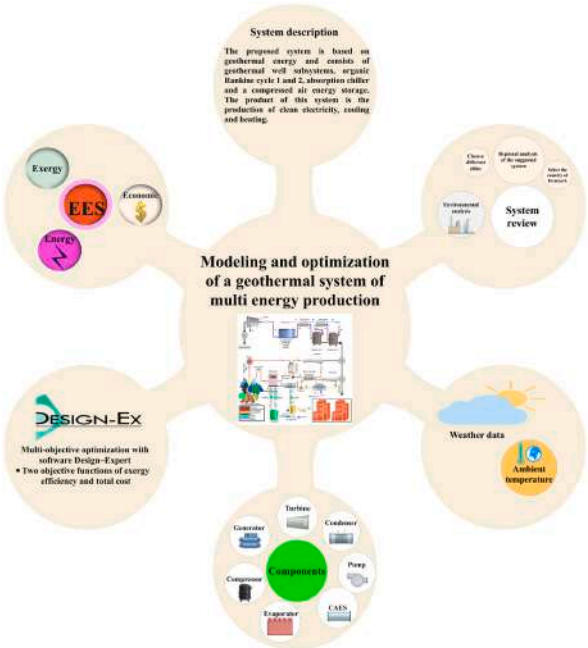


**Fig. 4.** Flowchart of the research method.

This methodology helps assess the system's performance, optimize its efficiency, and evaluate its environmental impact across different climates and locations.

It should be noted that the relations required for energy, exergy, and economic analysis of the system are presented in Appendix 1, 2, and 3.

## 4. Results and discussion

### 4.1. Validation

To validate the results of this study, a comparison was made with the results of Razmi et al. [30]. The study's validation process focused on the Compressed Air Energy Storage Subsystem (CAES). Table 2 presents the validation results of the current research, which demonstrate that this study holds good credibility in terms of its findings. This validation helps establish the reliability of the newly designed system introduced in this research.

### 4.2. Multi objective optimization

The response surface method is a set of mathematical techniques used to establish relationships between one or more response variables and several independent variables. The primary aim of employing response surface designs is to optimize a response (output variable) influenced by multiple independent variables (input variables). Optimizing a system using the response surface method typically involves the following five steps.

1. Selection of decision-making variables within the system based on screening studies and the study's objectives.
2. Choosing a test plan and conducting experiments based on the selected parameter space.
3. Conducting a mathematical and statistical analysis of the experimental data using appropriate polynomial functions.
4. Evaluating the fit of the model.
5. Determining optimal values for each variable under investigation.

In this optimization study, eleven input variables and two output variables were selected as the objective functions for optimization. The objective functions are Exergy Round Trip Efficiency (ERTE) and cost rate, chosen to enhance system performance and reduce economic costs. Multi-objective optimization is carried out using the response surface method (RSM), which ultimately yields the most optimal values for the objective functions and optimization variables.

Table 3 introduces the optimization variables and their respective ranges, providing the basis for the optimization process.

Optimizing the objective functions involved examining 160 runs to determine the final values of optimization variables, with the assistance of Design-Expert software. Response surface optimization was utilized to find the optimal combination of selected factors. As a result, after solving a hundred optimal points, the best solutions that the system can achieve were reported. Appendix 4 contains the results of these optimal points.

In Table 4, the outcome of the most optimal solution obtained through the response surface method is presented, with a Desirability value of 0.955. A Desirability value closer to 1 indicates a more acceptable solution.

Fig. 5 demonstrates the impact of optimization variables on the Exergy Round Trip Efficiency (ERTE) of the system. The objective of optimizing this function is to increase system efficiency. Enhancing system efficiency during optimization enables a reduction in carbon emissions and other pollutants generated by burning fossil resources to produce clean electricity. Efficiency and production power are directly related. The results reveal that the ERTE limit for the system in multi-objective optimization ranges from 20 % to 90 %. All the variables are optimized to achieve an ERTE of 77.981 %, which is the optimal value. In other words, by optimizing this objective function, it is possible to triple the system's performance. Gas turbine efficiency, turbine efficiency, evaporator pinch point temperature, pump efficiency, compressor efficiency, inlet temperature to the turbine, and inlet pressure to the compressed air energy storage are identified as the most influential design parameters. Increasing these parameters can have a significant impact on the ERTE of the system. It's worth noting that the gas turbine and the ORC turbine are the two main pieces of equipment in the system for power generation, and both operate using thermal energy. By improving the efficiency of the gas turbine and increasing turbine efficiency, the heat energy input to these devices increases. This results in increased output and enhanced system performance. The results indicate that, out of the 11 design parameters, these 7 parameters have the greatest influence on the system's ERTE.

**Table 2**
Validation results of the present study.

| Parameter | Present study | Reference [30] | Error |
|---|---|---|---|
| Maximum pressure of CAES (bar) | 20 | 20 | **0** |
| Minimum pressure of CAES (bar) | 6.667 | 6.667 | **0** |
| Inlet temperature of air turbine (K) | 1300 | 1300 | **0** |
| Power consumption of second compressor (kW) | 279.8 | 281.4 | **0.56** |
| Power consumption of third compressor (kW) | 280.1 | 281.8 | **0.60** |
| Output power of air turbine (kW) | 2279.3 | 2280 | **0.03** |

**Table 3**
**The** optimization variables and their ranges [10,26and31].

| Factor | Name | Low Level | High Level |
|---|---|---|---|
| **A** | Geothermal mass flow rate (kg/s) | 1 | 10 |
| **B** | T1 ($^0$C) | 190 | 220 |
| **C** | T4 ($^0$C) | 140 | 160 |
| **D** | T6 ($^0$C) | 60 | 90 |
| **E** | T8 ($^0$C) | 50 | 70 |
| **F** | Pinch point evaporator ($^0$C) | 5 | 9 |
| **G** | ORC turbine efficiency (%) | 0.7 | 0.95 |
| **H** | Pump efficiency (%) | 0.7 | 0.95 |
| **I** | Compressor efficiency (%) | 0.7 | 0.95 |
| **J** | Gas turbine efficiency (%) | 0.7 | 0.95 |
| **K** | $P_{28}$ (kPa) | 4500 | 5500 |

**Table 4**
The optimal results of objective functions and optimization variables.

| Parameter | Optimum point |
|---|---|
| Pump efficiency (%) | **0.803** |
| Compressor efficiency (%) | **0.888** |
| Gas turbine efficiency (%) | **0.894** |
| ORC turbine efficiency (%) | **0.89** |
| Pinch point evaporator ($^0$C) | **5.984** |
| T8 ($^0$C) | **65.49** |
| T6 ($^0$C) | **66.771** |
| T4 ($^0$C) | **152.999** |
| T1 ($^0$C) | **206.689** |
| Geothermal mass flow rate (kg/s) | **3.029** |
| P28 (kPa) | **4779.956** |
| ERTE (%) | **77.981** |
| Cost rate ($/h) | **5.489** |

Fig. 6 illustrates the investigation of the impact of optimization variables on the system cost rate. The objective of optimizing this function is to minimize system costs because a multi-production system should not only deliver satisfactory performance but also maintain low economic costs. The results indicate that the system cost limit in multi-objective optimization falls within a range of 3.717 $/h to 40 $/h. All the variables are optimized to achieve a system cost rate of 5.489 $/h, which represents the optimal value. In other words, optimizing this objective function can significantly reduce system costs. Among the design parameters, compressor efficiency, inlet temperature to evaporator, inlet temperature to turbine 1, inlet temperature to turbine 2, geothermal mass flow rate, and inlet temperature to pump are identified as the most influential factors. Increasing these parameters can have a substantial impact on reducing the system's cost rate. The results reveal that, out of the 11 design parameters, these 6 parameters have the greatest influence on the system's cost rate.

### *4.3. Forecasting*

To forecast and estimate the behavior of the optimized objective functions discussed in the preceding section, data from the 100 optimized runs provided in Appendix 4 are utilized for prediction. The performance of the two objective functions is individually analyzed using the genetic-regression algorithm. Genetic algorithms employ concepts from evolutionary biology, including heredity, biological mutation, and the principles of selection as described by Darwin, to determine the most suitable formula for prediction or model fitting. Genetic algorithms frequently offer a robust alternative to regression-based prediction methods. For the sake of simplicity, specific symbols were assigned to represent the design parameters, as outlined in Table 5.

Equation 5 represents the regression relationship for the cost rate objective function, and the coefficients of this equation are provided in Table 6. This equation models the relationship between the cost rate and the relevant factors, and the coefficients in Table 6 specify the values associated with each term in the equation. These coefficients are crucial for calculating the cost rate based on the input factors considered in the regression model.

$$\begin{aligned} \textit{Cost rate} = (((a1{*}D + ((((a2{*}G{*}a3{*}LN(a4{*}A) - (a5{*}B + a3)) \,/\, (((a6{*}A + a7{*}E) \,/\, ((a8 \,/\, (a9{*}C) - a10)) - (a6{*}\$A1 + a7{*}\$E1))) \\ + ((a8 - a10){*}LN(-a11{*} - a12{*} - a13{*} - a14{*}D) - (-a18{*}H - a15) \,/\, ((-a16 - a17){*} - 18 \,/\, (a19{*}J) \\ \,/\, ((a7{*}C + a20)))) - a2{*}K1{*}a3) + a6{*}C) - (a22{*}B + a23)){*} - a23 + a24) \end{aligned} \quad (5)$$

Equation (6) presents the regression relationship for the Exergy Round Trip Efficiency (ERTE) objective function, and the coefficients of this equation are detailed in Table 7. This equation serves as a mathematical representation of the relationship between the ERTE and its relevant factors, and the coefficients in Table 7 provide specific values for each term in the equation, allowing for the

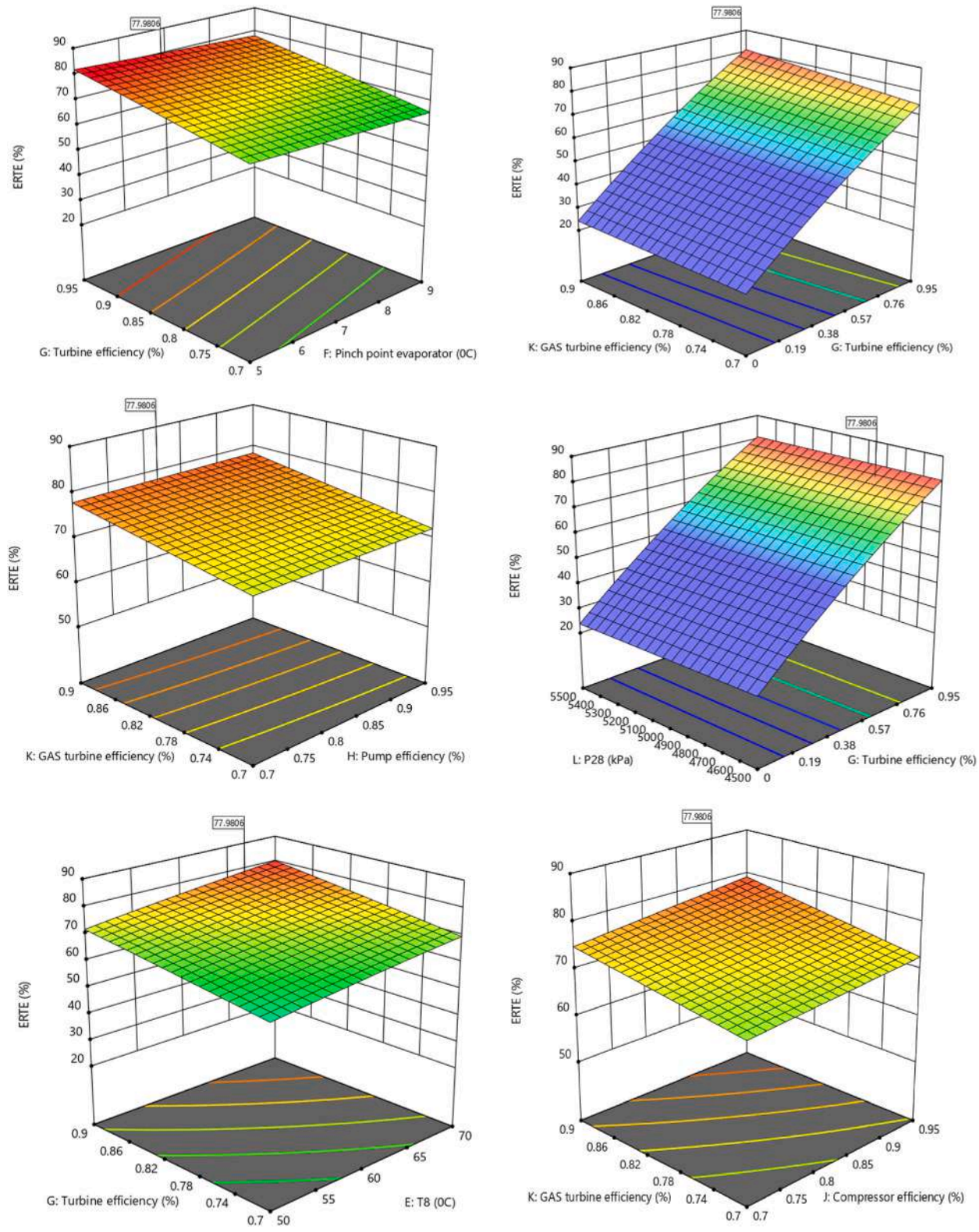


**Fig. 5.** The effect of decision variables on ERTE.

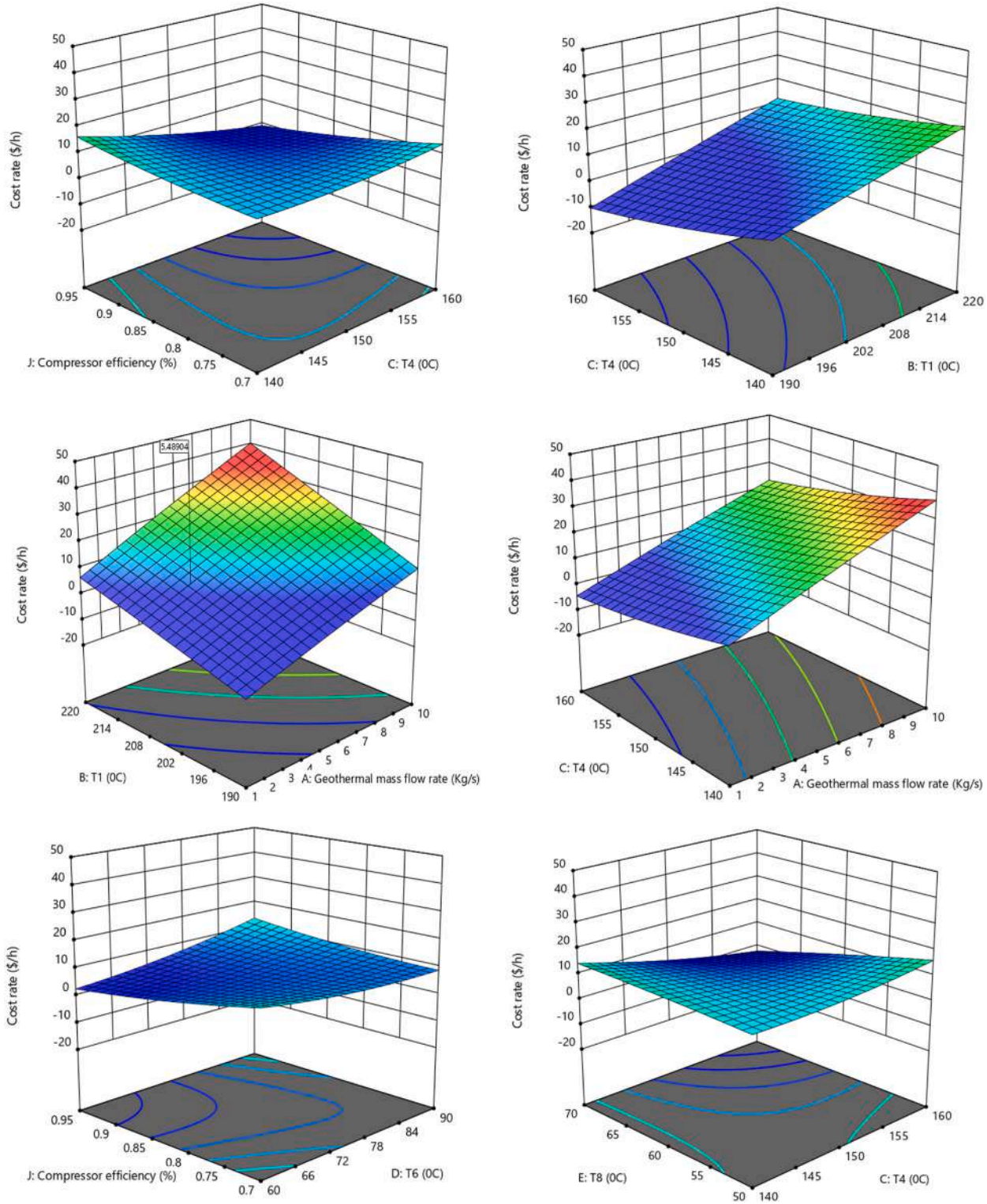


**Fig. 6.** The impact of decision variables on the cost rate.

**Table 5**
Simplification of regression relationships.

| Decision variables | symbol |
|---|---|
| **Geothermal rate (kg/s)** | A |
| **T1 ($^0$C)** | B |
| **T4 ($^0$C)** | C |
| **T6 ($^0$C)** | D |
| **T8 ($^0$C)** | E |
| **Pinch point evaporator ($^0$C)** | F |
| **ORC turbine efficiency (%)** | G |
| **Pump efficiency (%)** | H |
| **Compressor efficiency (%)** | I |
| **Gas turbine efficiency (%)** | J |
| **$P_{28}$ (kPa)** | K |

**Table 6**
Coefficients of cost rate regression equation.

| Coefficient | Valve | Coefficient | Valve |
|---|---|---|---|
| $a_1$ | 0.45 | $a_{13}$ | **17.37** |
| $a_2$ | 1.15 | $a_{14}$ | **0.46** |
| $a_3$ | 18.56 | $a_{15}$ | **4.47** |
| $a_4$ | 1.21 | $a_{16}$ | **7.25** |
| $a_5$ | 10.7 | $a_{17}$ | **9.46** |
| $a_6$ | 2.38 | $a_{18}$ | **10.97** |
| $a_7$ | 1.02 | $a_{19}$ | **2.09** |
| $a_8$ | 14.13 | $a_{20}$ | **0.80** |
| $a_9$ | 0.95 | $a_{21}$ | **1.49** |
| $a_{10}$ | 6.60 | $a_{22}$ | **5.38** |
| $a_{11}$ | 13.93 | $a_{23}$ | **0.25** |
| $a_{12}$ | 7.79 | $a_{24}$ | **16.48** |

calculation of the ERTE based on these factors.

$$ERTE = (b1*H*((b2*H - b3*H) - b4*G* - b5)*(( - b3*F*b6*A + ((b7 - (b4*G - (-b8 + b9*C))) - b1*H*(b10*D - (-b8 + b9*C)))) - (b2*H - b3*H)* - b5)*( - b11/((b2*H - b10*D1)) - b1*H*(b10*D - b12*b13*F))*(((b14*b15*E + (-b8 + b9*C)) - ((((b10*D - ( - b16/(-b8) + b9*C)) - (b2*H* b17*B - (-b8 + b9*C))) + b6*A) - b17)) - b18)* - b19E + b20) \quad (6)$$

Fig. 7 presents the prediction of the behavior of the three objective functions: Exergy Round Trip Efficiency (ERTE) and cost rate, using two modes of testing and training, along with an evaluation of the objective. This diagram provides insights into the behavior of decision variables during the optimization process and illustrates the two modes of testing and training used for model validation. In this graph, 80 % of the data was allocated for training, while 20 % was designated for testing. This data partitioning allows for the assessment of model performance. The diagram features three modes:

- ❖ Objective Function Value: This mode represents the actual objective function values.
- ❖ Objective Function Prediction in Testing Mode: This mode shows the predicted values of the objective functions during testing.
- ❖ Objective Function Prediction in Training Mode: This mode displays the predicted values of the objective functions during training.

**Table 7**
The coefficients of the ERTE regression equation.

| Coefficient | Valve | Coefficient | Valve |
|---|---|---|---|
| $b_1$ | 0.17 | $b_{11}$ | **16.58** |
| $b_2$ | 0.98 | $b_{12}$ | **0.82** |
| $b_3$ | 0.48 | $b_{13}$ | **1.39** |
| $b_4$ | 0.69 | $b_{14}$ | **13.77** |
| $b_5$ | 7.35 | $b_{15}$ | **1.66** |
| $b_6$ | 2.29 | $b_{16}$ | **8.53** |
| $b_7$ | 12.32 | $b_{17}$ | **0.46** |
| $b_8$ | 9.87 | $b_{18}$ | **11.27** |
| $b_9$ | 2.03 | $b_{19}$ | **3.44** |
| $b_{10}$ | 2.60 | $b_{20}$ | **57.14** |

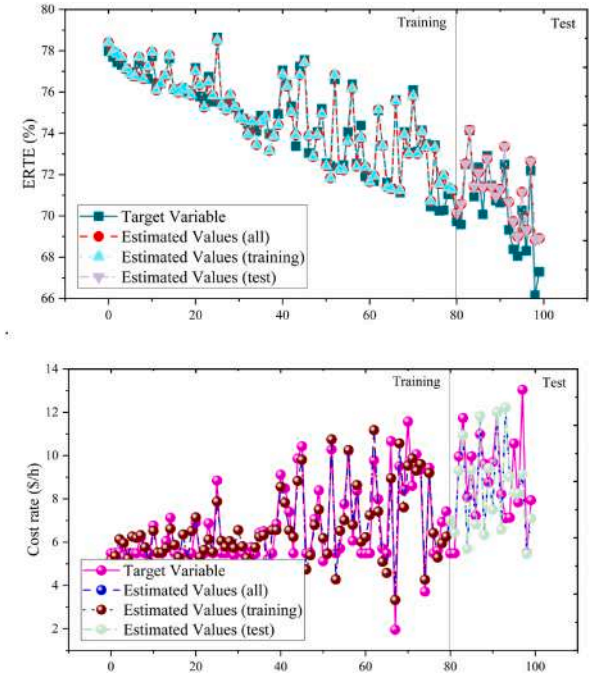


**Fig. 7.** Predicting the behavior of the investigated objective functions.

The primary goal of this visualization is to assess how well the model predicts the objective function values in both testing and training phases. The objective function line represents the ideal values, and the model's performance is evaluated based on how closely the predicted values align with this ideal line. Fig. 7 shows the results of the objective function prediction process, which as the horizontal axis shows, the objective function data has 100 points. The 100 points examined to predict the objective functions are the same optimization data extracted from the response surface optimization method as presented in Appendix 4. This data is divided into two parts, 20 % of which is selected for testing and 80 % of which is chosen for training.

Fig. 8 depicts the estimation of the flow functions for the objective functions of Exergy Round Trip Efficiency (ERTE) and cost rate. This visualization comprises two axes: the actual values of the objective function are plotted on the horizontal axis, while the estimated values of the cost objective function are displayed on the vertical axis of the diagram. In this graph, you can observe various data points representing the objective function values throughout the solution process. The proximity of the actual and estimated values is a key point of interest. When the actual and estimated values closely align or overlap, it signifies that the modeling has performed well and accurately predicted the objective functions. This alignment represents the best results for both the ERTE and cost rate, indicating a successful modeling and optimization process. This information was calculated using genetic algorithm and linear regression, which was extracted by HeuristicLab software and presented in the form of a graph.

Fig. 9 presents a histogram of three objective functions: Exergy Round Trip Efficiency (ERTE) and cost rate, which are the two primary outcomes for both the training and testing phases. This histogram illustrates the distribution of these objective functions across various categories. In this visualization, each column's height represents the frequency of the objective function falling within a specific category. The horizontal axis displays the values of the objective function, while the vertical axis indicates the percentage frequency of each category.

This histogram provides a visual representation of the distribution of ERTE and cost rate values in the training and testing processes, offering insights into the variability and frequency of different outcomes for these key performance metrics.

### *4.4. Economic analysis*

Fig. 10 provides a breakdown of the total cost rate distribution for the proposed system, including the individual cost rates for the main system components. The system components are categorized into three main parts: ORC 1, ORC 2, and the compressed air energy storage unit. The total cost of the system is calculated to be 12.7087 $/h. The highest cost within the system is associated with the Compressed Air Energy Storage (CAES) unit, accounting for 5.0008 $/h. This is followed by the ORC 1 unit with a cost rate of 4.7564 $/h and the ORC 2 unit with a cost rate of 2.5615 $/h. The CAES unit and the gas turbine are considered relatively expensive technologies, resulting in the highest cost rates among the system components. In contrast, the absorption chiller unit has the lowest cost rate in the system, amounting to 0.39 $/h. Among the equipment components, Turbine 1 has a cost rate of 4.402 $/h, the gas turbine is associated with a cost rate of 2.969 $/h, and Turbine 2 has a cost rate of 2.431 $/h. These equipment components are considered relatively expensive. In contrast, the pumps have the lowest cost rates among all the equipment used in the system.

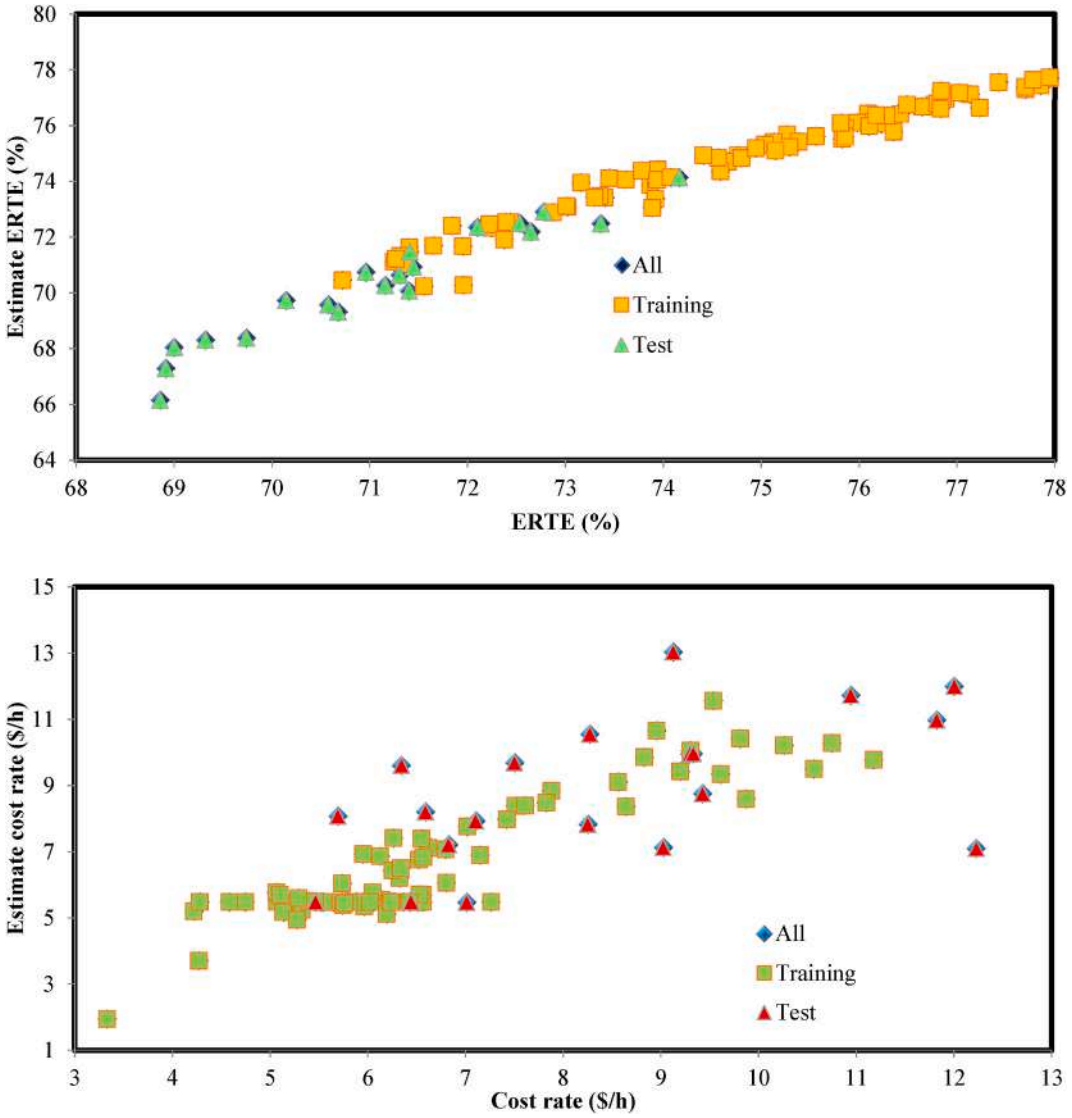


**Fig. 8.** Estimation of the flow functions of the investigated objective functions.

This analysis provides insights into the cost distribution of the proposed system and highlights the components with the highest and lowest associated costs.

### *4.5. Case study*

A feasibility study was conducted to assess the potential implementation of the proposed system in Denmark, a European country known for its favorable geothermal conditions. For this purpose, ten different cities in Denmark were selected, each with its own unique climate and weather conditions. Denmark is recognized as having significant geothermal potential, making it a promising region for harnessing geothermal energy.

The chosen cities are considered to be among the best and most promising geothermal areas in Denmark. These cities include Aalborg, Arhus, Ars, Flakkeberg, Foulum, Holbaek, Horsens, Copenhagen, Roskilde, and Odense. Fig. 11 likely provides a geothermal map of Denmark, highlighting regions with geothermal potential. The study aimed to evaluate the feasibility of implementing the proposed system in each of these cities to harness geothermal energy efficiently.

Fig. 12 presents the daily changes in the average ambient temperature throughout the year for the study cities in Denmark. These data are plotted for all 365 days of the year. The results indicate that the average temperatures in the studied cities vary between −10 °C and 25 °C. The highest ambient temperatures are observed during the summer months of June, July, and August. This information provides a comprehensive overview of the temperature variations in these cities, which is vital for assessing the performance and feasibility of various energy systems, including geothermal and gas turbine systems, as discussed earlier.

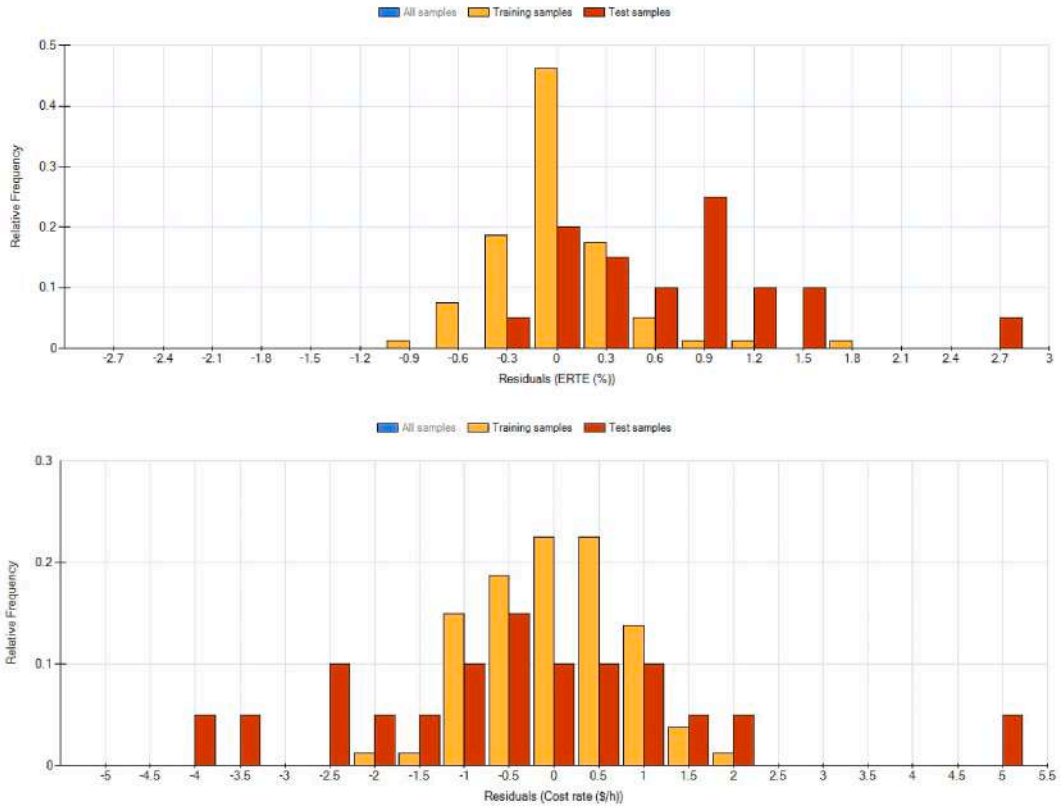


**Fig. 9.** The histogram diagram of the investigated objective functions.

Fig. 13 depicts the daily variations in power production from the dual Organic Rankine Cycle (ORC) in response to changes in weather parameters. The ORC turbine is primarily responsible for power generation in the system, and variations in environmental conditions can directly impact the system's power output. Comparing the system's performance in the studied cities reveals that the system performs most effectively in the cities of Foulum, Ars, and Arhus.

The results indicate that as the ambient temperature in the cities increases, particularly in warmer regions, the performance of the dual ORC system tends to decrease. Therefore, rising ambient temperatures have a negative effect on the performance of the dual ORC system, making it more suitable for deployment in cooler regions. This information is valuable for selecting the optimal locations for implementing the dual ORC system, where it can operate at peak efficiency.

Fig. 14 displays the daily variations in power production from the gas turbine in response to changes in weather parameters. An increase in ambient temperature has a negative impact on the performance of the gas turbine. A comparison of the system's performance in the studied cities reveals that the gas turbine performs most effectively in the cities of Foulum, Ars, Arhus, and Roskilde, which are the coldest regions among the selected cities.

As the ambient temperature in the region rises, the production performance of the gas turbine tends to decrease. Consequently, the cities with higher ambient temperatures, like Holbaek, experience lower power production from the gas turbine. This information is crucial for selecting the most suitable locations for deploying the gas turbine system, optimizing its performance in cooler regions.

Fig. 15 illustrates the daily variations in the total system power production, which includes the combined power generated by the turbines and gas turbine, minus the power consumed by the Compressed Air Energy Storage (CAES) unit compressors. The results demonstrate that an increase in ambient temperature negatively impacts the performance of the gas turbine and the organic turbine. Therefore, regions with colder climates are more suitable for implementing the system because the performance of these turbines is less affected by temperature changes. Comparing the system's performance across the study cities reveals that the system performs most effectively in the cities of Foulum, Ars, Arhus, and Roskilde, respectively. As the temperature in the area increases, the overall system performance tends to decrease. This information is essential for selecting the most favorable locations for deploying the system, optimizing its performance in cooler regions.

Fig. 16 displays the daily variations in heating production from the system in response to changes in the weather parameters of the cities. The heating is generated using the heat output from the Organic Rankine Cycle (ORC) condenser. As the ambient temperature rises and the heat input to the system increases, the amount of heat lost from the system also increases. Consequently, an increase in ambient temperature leads to greater heating production.

Comparing the system's performance across the study cities reveals that the system achieves the highest heating production in cities with warmer climates, characterized by higher ambient temperatures. Specifically, the cities of Odense and Copenhagen, due to their

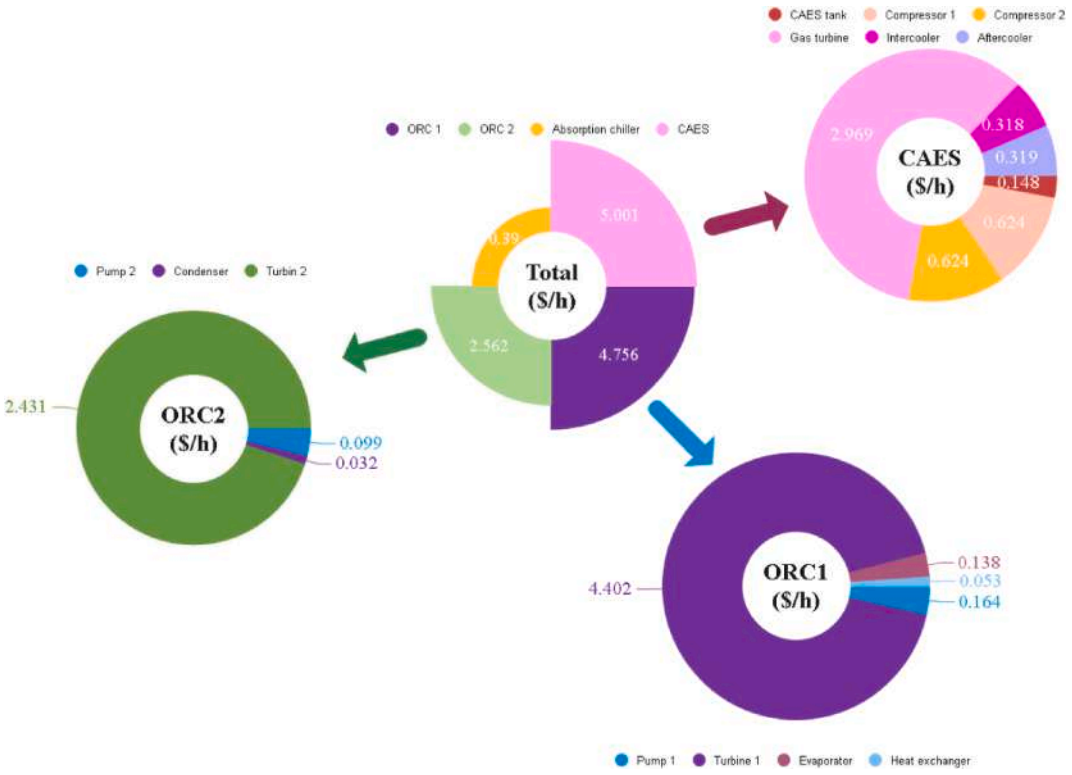


**Fig. 10.** The cost rate of units and components of the system in the optimal state.

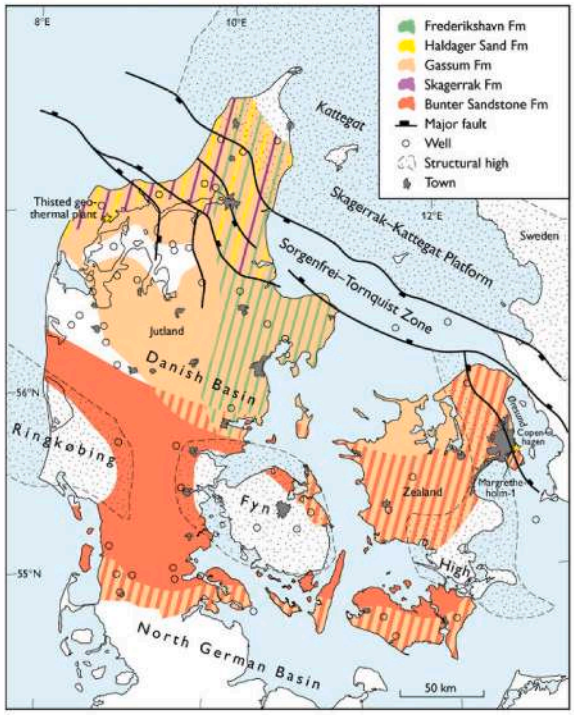


**Fig. 11.** Geothermal map of Denmark.

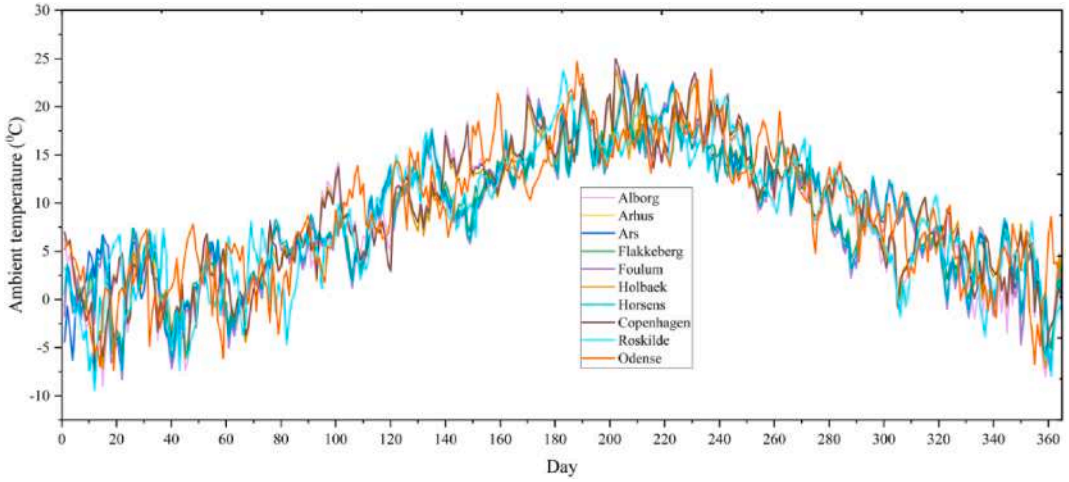


**Fig. 12.** Changes in the average ambient temperature of the study cities in Denmark throughout the year.

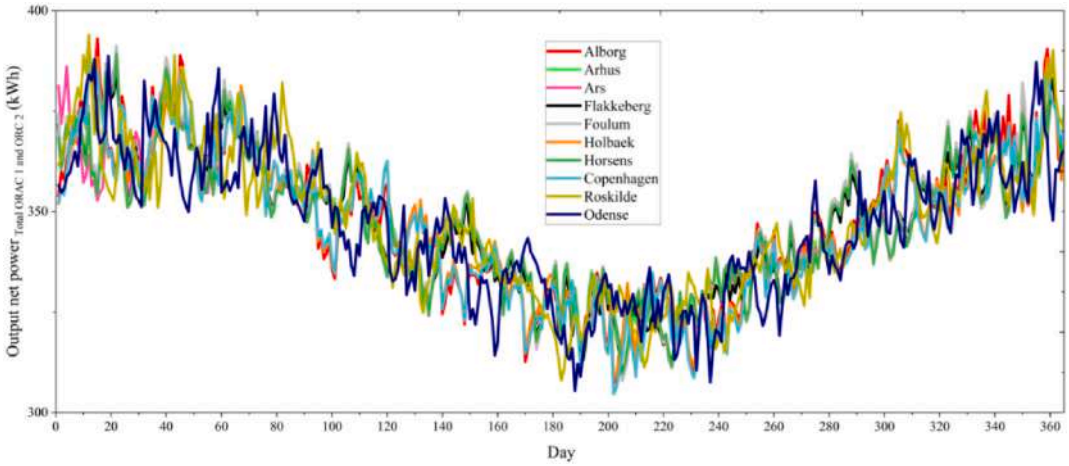


**Fig. 13.** Changes in the production power of the double ORC of the study cities in Denmark daily.

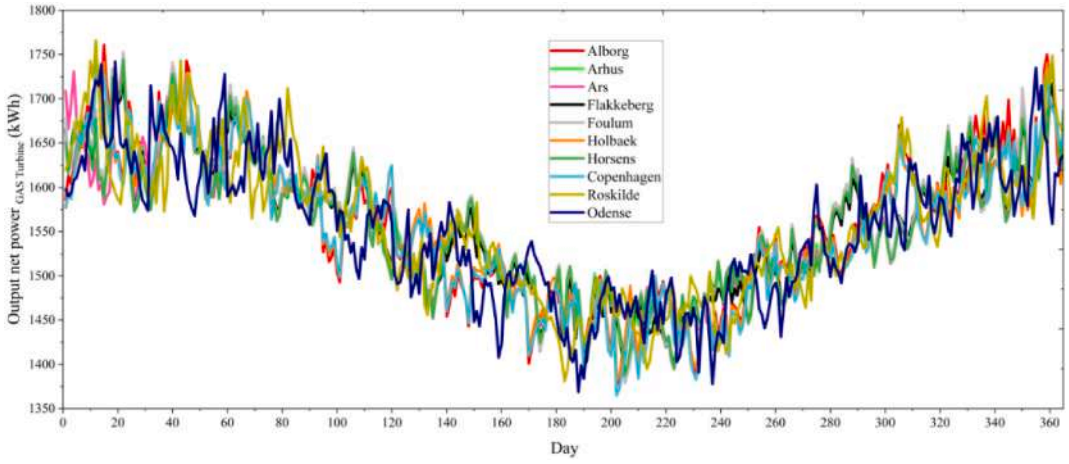


**Fig. 14.** Changes in the production power of the gas turbine in the study cities of Denmark daily.

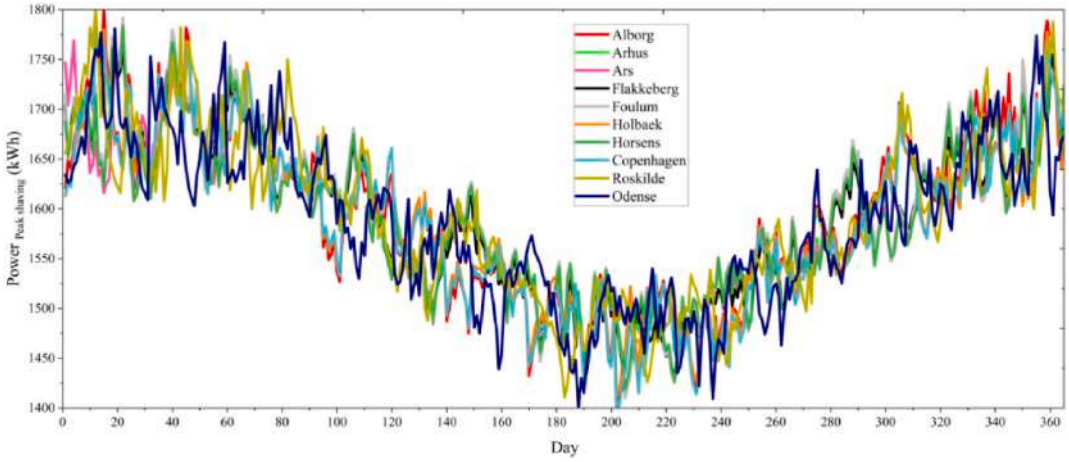


**Fig. 15.** Changes in the production power of the system during the peak time of the study cities in Denmark daily.

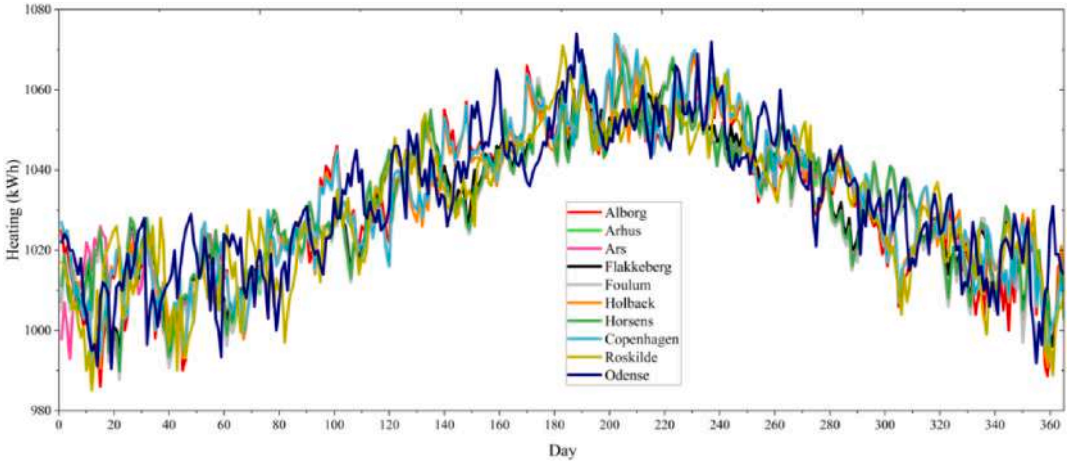


**Fig. 16.** Changes in the amount of heating produced by the system in the study cities of Denmark daily.

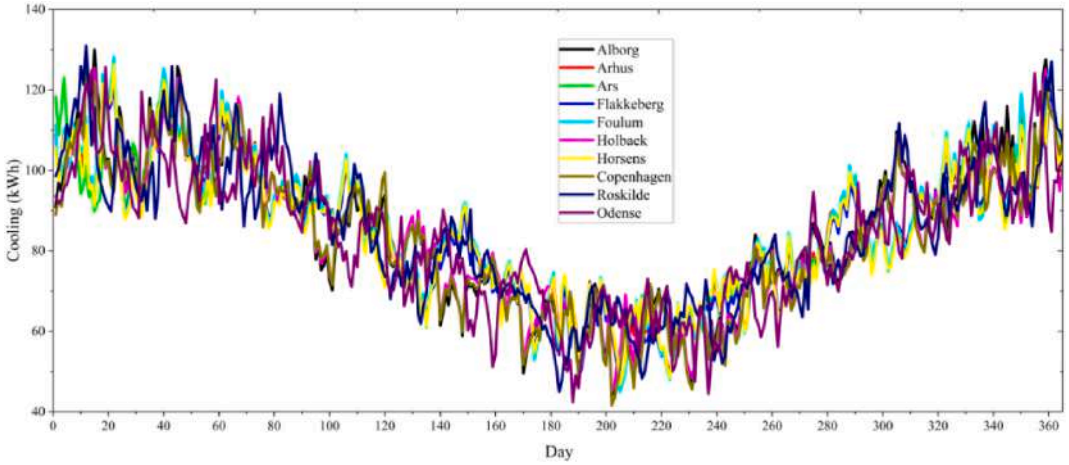


**Fig. 17.** Production cooling changes in the study cities of Denmark daily.

elevated ambient temperatures, exhibit the most substantial heating production. In contrast, selecting colder areas, such as the cities of Foulum, Ars, and Arhus, reduces the amount of heating generated by the system. This information is valuable for optimizing heating production based on regional climate conditions.

Fig. 17 examines the cooling production rate of the system in the study cities of Denmark in response to changes in ambient temperature. The production of cooling is facilitated by the absorption chiller within the system. The results indicate that an increase in ambient temperature leads to a reduction in the system's cooling production rate. The highest cooling production rate is observed during the winter months, particularly in January and February. Among the study cities, Foulum, characterized by a colder climate, exhibits the highest cooling production rate. In contrast, the cities of Odense and Copenhagen, with warmer climates, have the lowest cooling production rates. This information highlights the impact of climate conditions on the cooling production capacity of the system and underscores the importance of selecting suitable locations for optimizing cooling production based on regional temperature variations.

Fig. 18 presents the daily average changes in the Exergy Round Trip Efficiency (ERTE) of the system across the study cities in Denmark. Exergy efficiency, production power, and cost rate are interconnected parameters in the system. Therefore, variations in production power correspond to similar changes in the ERTE of the system. Consequently, the cities with the highest ERTE correspond to the most optimal study cities. This figure provides valuable insights into the system's exergy efficiency and its daily variations across the different cities under consideration.

Fig. 19 displays the daily average changes in system cost rates across Danish cities. Cost rate and production capacity are directly related. Consequently, variations in production capacity lead to similar changes in the system's cost rate. An increase in production capacity results in higher maintenance costs for the system, and vice versa. When comparing the system's performance in the study cities, it becomes evident that the cities with the highest production capacity and Exergy Round Trip Efficiency (ERTE) tend to have the highest cost rates. This figure provides insights into the relationship between production capacity and system cost, helping to identify optimal locations for system deployment based on cost considerations.

### 4.6. Best study city

Fig. 20 compares the total annual production capacity of the 10 study cities in Denmark under two scenarios: one with peak consumption and another without peak consumption. The results indicate that the city of Foulum stands out as the best-performing city with the highest production capacity, while the city of Odense exhibits the lowest production capacity.

In Fig. 21, it is shown that the highest cost rate is associated with the city of Foulum, which has the highest rate of power generation. In contrast, the city of Odense has the lowest cost rate, and it also has the lowest power generation rate among the cities in the study.

The aim of this research is to select a city that achieves a balance between high production capacity and reasonable production cost, optimizing the system's performance based on these criteria.

### 4.7. Environmental analysis

Fig. 22 provides a quantitative assessment of the environmental advantages offered by the integrated organic waste and wastewater management system designed for Aarhus, Denmark. The analysis compares the environmental costs associated with conventional electricity production to the potential benefits of implementing the proposed system. In conventional power plants, the production of 1 MW-hour of electricity typically results in the emission of approximately 0.204 tons of CO2. Each ton of CO2 emitted is associated with an estimated environmental cost of $24. These environmental costs arise from the negative impacts of greenhouse gas emissions on the climate, ecosystems, and human health. By implementing the integrated system designed for Aarhus, it is possible to

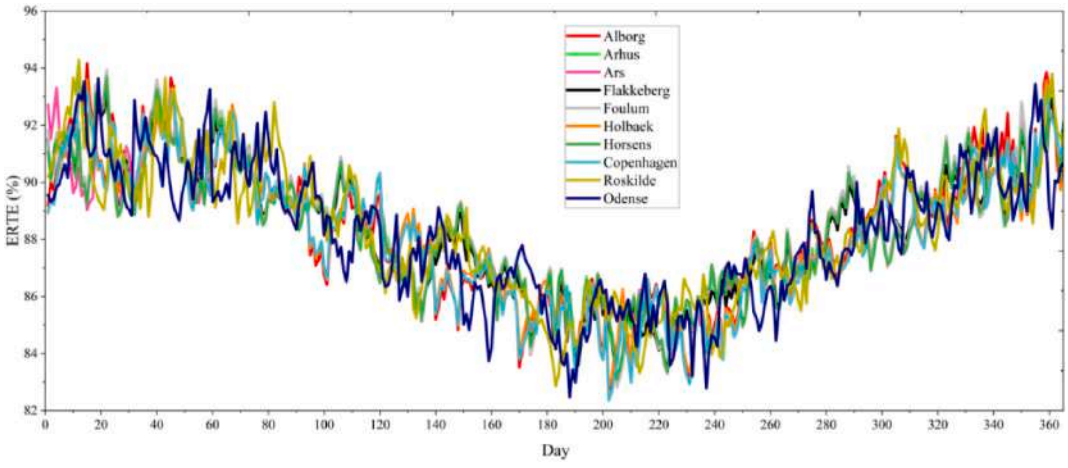


**Fig. 18.** Average hourly changes of ERTE of study cities in Denmark daily.

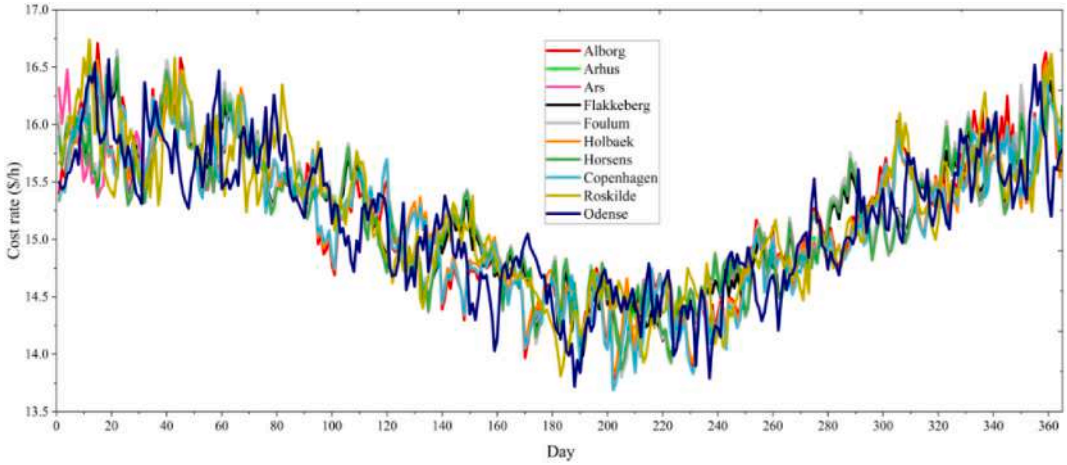


**Fig. 19.** Average hourly cost rate changes of study cities in Denmark daily.

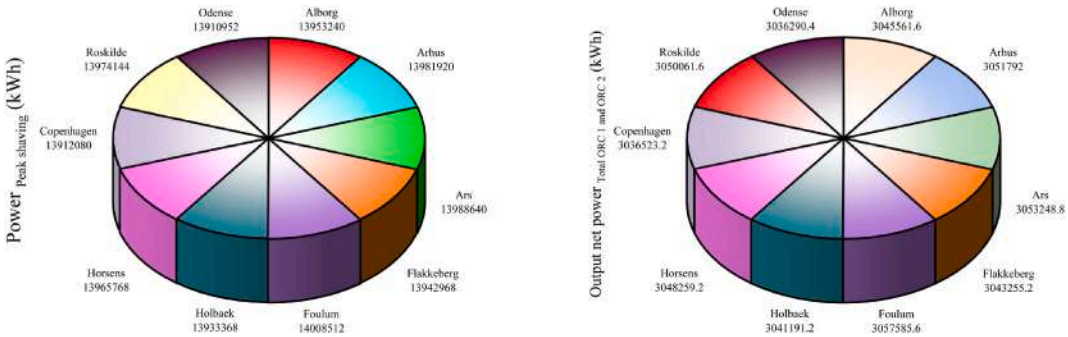


**Fig. 20.** The total annual production capacity of the study cities in Denmark.

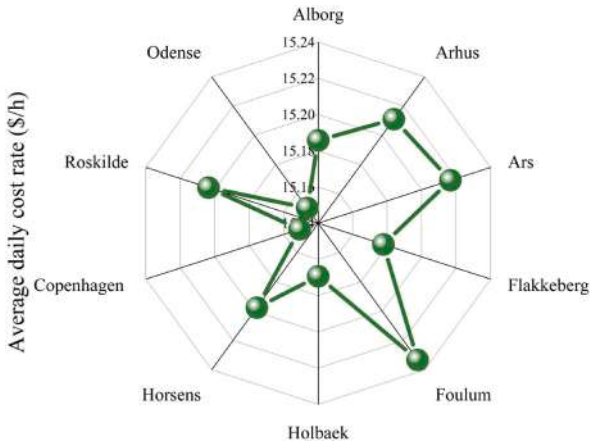


**Fig. 21.** Annual average cost rate of Danish study cities.

significantly reduce these environmental costs, contributing to environmental preservation and the expansion of green spaces and plant life. The system's ability to mitigate CO2 emissions and associated environmental costs highlights its potential to promote sustainability and ecological well-being. To further quantify the system's environmental benefits, an average price of $4940 per hectare was considered for non-settlement water habitat. This valuation of ecosystem services emphasizes the economic value of preserving and enhancing natural habitats, which provide a range of benefits to society [32,33], such as water purification, flood regulation, and biodiversity conservation [34,35]. while considering uncertainties [36].

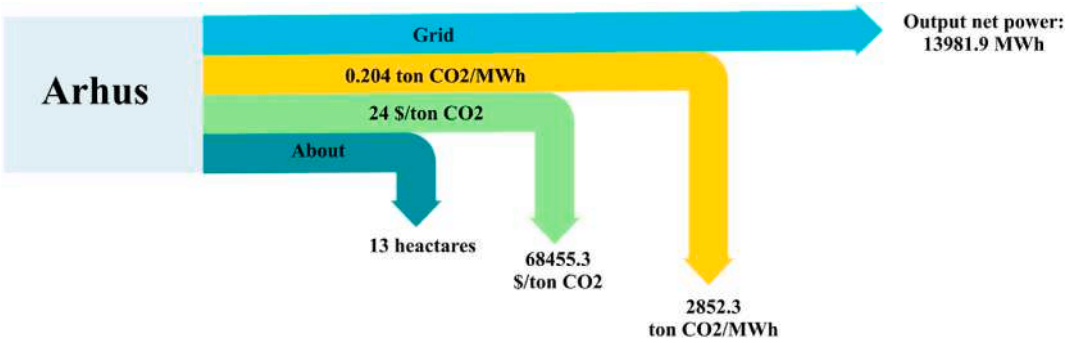


**Fig. 22.** Environmental performance of the system in Aarhus city.

## 5. Conclusion

In this research, a comprehensive analysis of a multi-production system based on geothermal energy was conducted, along with a feasibility study for implementing the system in Denmark. The primary goals were to maximize system efficiency and minimize associated costs. The studied system comprises various components, including geothermal subsystems, ORC 1 and 2, a compressed air energy storage source, and an absorption chiller. The system employs refrigerant R123 and ammonia in the ORC.

To optimize the system's performance, the Response Surface Method and Design-Expert software were employed, with a focus on two key objective functions: Exergy Round Trip Efficiency (ERTE) and cost rate. Various design variables were considered for optimization, encompassing parameters like turbine and pump inlet temperatures, geothermal mass flow rate, turbine and pump efficiencies, compressor efficiency, gas turbine efficiency, inlet pressure to the CAES tank, and the pinch point temperature of the evaporator:

The key findings of this research include.

- Achieving an optimal ERTE value of 77.98 %.
- Attaining the most favorable cost rate of 5.48 $/h.
- Identifying that the highest cost rate is attributed to the compressed air energy storage unit, followed by ORC 1 and ORC 2.
- Selecting 10 study cities in Denmark for the feasibility analysis.
- Concluding that Aarhus is the most suitable city for system deployment, considering both technical and economic factors.
- The environmental results showed that with the annual production of 13981.9 MW of electricity in Aarhus City, it is possible to help reduce $CO_2$ emissions by 2853.2 tons of $CO_2$/year.
- The environmental analysis showed that the ecological costs of 68,455.3 $/year could be avoided by setting up the proposed system in Aarhus.
- Demonstrating that implementing the proposed system in Aarhus, Denmark, would lead to the expansion of 13 ha of green space.
- These findings emphasize the efficiency, cost-effectiveness, and environmental benefits of the proposed geothermal system, particularly when implemented in the city of Aarhus.

## 6. Suggestions

In this section, suggestions are given to the researchers to complete the present work:

- Today, the energy supply of buildings by renewable systems should be the attention of researchers, because fossil energies are running out and have much environmental pollution.
- The use of cooling and heating production units in the current system, such as a compression chiller, can complete the proposed system for providing energy consumption in residential buildings.
- The use of a freshwater production unit such as reverse osmosis can be suitable for use in areas where there is access to salty sea water and there is little freshwater.
- Combining the proposed system with photovoltaic panels or wind turbines can help improve system performance and increase system stability.
- Using the neural network optimization method and combining it with the optimization method in the current research can help to improve the accuracy of the system optimization.
- The use of batteries can be used to store more energy and use in sensitive times and conditions.

## CRediT authorship contribution statement

**Ehsanolah Assareh:** Writing – review & editing, Writing – original draft, Visualization, Validation, Supervision, Software,

Resources, Project administration, Methodology, Investigation, Formal analysis, Data curation, Conceptualization. **Siamak Hoseinzadeh:** Writing – review & editing, Writing – original draft, Visualization, Validation, Supervision, Resources, Methodology, Investigation, Funding acquisition, Formal analysis, Conceptualization. **Abolfazl Karami:** Writing – original draft, Visualization, Validation, Software, Resources, Methodology, Investigation, Formal analysis, Data curation, Conceptualization. **Hassan Bazazzadeh:** Writing – review & editing, Writing – original draft, Visualization, Resources, Project administration, Methodology, Investigation, Funding acquisition, Formal analysis, Conceptualization. **Daniele Groppi:** Writing – review & editing, Visualization, Validation, Methodology, Investigation, Formal analysis, Conceptualization. **Davide Astiaso Garcia:** Writing – review & editing, Project administration, Methodology, Investigation, Funding acquisition, Formal analysis, Conceptualization.

## Declaration of competing interest

The authors declare that they have no known competing financial interests or personal relationships that could have appeared to influence the work reported in this paper.

## Appendix 1

In Appendix 1, the basic relations for energy, exergy, and economic analysis of the system are presented.

*Appendix 1. Thermodynamic analysis*

| Basic relationships | Relation | Reference |
|---|---|---|
| *Law of survival of the crime* | $\sum_k \dot{m}_i - \sum_k \dot{m}_e = \frac{dm_{cv}}{dt}$ | [37] |
| *Law of conservation of energy* | $\dot{Q} - \dot{W} + \sum_i \dot{m}_i \left(h_i + \frac{v_i^2}{2} + gZ_i\right) - \sum_e \dot{m}_e \left(h_e + \frac{v_e^2}{2} + gZ_e\right) = \frac{dE_{cv}}{dt}$ | [38] |
| *Exergy Balance* | $\dot{E}x_Q + \sum_i \dot{m}_i (ex_i) = \sum_e \dot{m}_e (ex_e) + \dot{E}x_w + \dot{E}x_D$ | [39] |
| *Physical Exergy* | $\dot{E}x_{ph} = \sum_i \dot{m}_i ((h_i - h_0) - T_0 (s_i - s_0))$ | [39] |
| *Cost Rate* | $\dot{Z} = \frac{Z \times CRF \times \varphi}{T}$ | [40] |
| *Capital Recovery Factor* | $CRF = \frac{k(1+k)^n}{(1+k)^n - 1}$ | [41] |

## Appendix 2

*Appendix 2. Energy balance of the system*

| System components | Relation | Reference |
|---|---|---|
| *Turbine 1* | $W_{turbine\ 1} = \dot{m}_4 \times (h_4 - h_5)$ | [42] |
| *Turbine 2* | $W_{turbine\ 2} = \dot{m}_8 \times (h_8 - h_9)$ | [42] |
| *Pump 1* | $W_{pump1} = \dot{m}_6 \times (h_7 - h_6)$ | [42] |
| *Pump 2* | $W_{pump2} = \dot{m}_{10} \times (h_{11} - h_{10})$ | [42] |
| *Evaporator* | $Q_{Evaporator} = \dot{m}_1 \times (h_1 - h_2)$ | [43] |
| *Condenser* | $Q_{condenser} = \dot{m}_9 \times (h_9 - h_{10})$ | [43] |
| *Heat exchanger* | $Q_{HEX} = \dot{m}_5 \times (h_5 - h_6)$ | [43] |
| *Intercooler* | $Q_{Intercooler} = \dot{m}_{25} \times (h_{25} - h_{26})$ | [26] |
| *Aftercooler* | $Q_{Aftercooler} = \dot{m}_{27} \times (h_{27} - h_{28})$ | [26] |
| *ORC1 power* | $W_{net,ORC\ 1} = W_{turbin1} + W_{pump\ 1}$ | [43] |
| *ORC2 power* | $\dot{W}_{net,ORC\ 2} = \dot{W}_{turbin2} + \dot{W}_{pump\ 2}$ | [43] |
| *Compressor 1* | $W_{Comp\ 1} = \dot{m}_{24} \times (h_{25} - h_{24})$ | [26] |
| *Compressor 2* | $W_{Comp\ 2} = \dot{m}_{26} \times (h_{27} - h_{26})$ | [26] |
| *Compressed air energy storage* | $W_{CAES} = W_{Comp\ 1} + W_{Comp\ 2}$ | [26] |
| *Gas turbine* | $W_{GT} = \dot{m}_{33} \times (h_{33} - h_{34})$ | [26] |
| *Heater* | $Q_{heater} = \dot{m}_{32} \times (h_{33} - h_{32})$ | [26] |

## Appendix 3

*Appendix 3. Cost balance*

| System components | Relation | Reference |
|---|---|---|
| *Turbine 1* | $Z_{\text{Turbine 1}} = 4750 \times \left(\left(W_{\text{turbine}}{}^{0.75}\right) + 60 \times \left(W_{\text{turbine}}{}^{0.95}\right)\right)$ | [42] |
| *Turbine 2* | $Z_{\text{Turbine 2}} = 4750 \times \left(\left(W_{\text{turbine}}{}^{0.75}\right) + 60 \times \left(W_{\text{turbine}}{}^{0.95}\right)\right)$ | [42] |
| *Pump 1* | $Z_{\text{Pump1}} = 3500 \times \left(W_{\text{Pump1}}{}^{0.41}\right)$ | [42] |
| *Pump 2* | $Z_{\text{Pump2}} = 3500 \times \left(W_{\text{Pump2}}{}^{0.41}\right)$ | [42] |
| *Condenser* | $Z_{\text{Cond}} = 1773 \times \dot{m}_9$ | [43] |
| *Evaporator* | $Z_{\text{Evap}} = 276 \times \left(A_{\text{Evap 1}}{}^{0.88}\right)$ | [43] |
| *Heat exchanger* | $Z_{\text{HEX}} = 12000 \times \left(\frac{A_{\text{HX}}}{100}\right)^{0.88}$ | [43] |
| *Intercooler* | $Z_{\text{Intc}} = 12000 \times \left(\frac{A_{\text{Intc}}}{100}\right)^{0.6}$ | [26] |
| *Aftercooler* | $Z_{\text{Aftc}} = 12000 \times \left(\frac{A_{\text{Aftc}}}{100}\right)^{0.6}$ | [26] |
| *Compressor 1* | $Z_{\text{Comp1}} = \frac{(71.1 \times \dot{m}_{24})}{(0.9 - \eta_{\text{Compressor}}) \times ((P_{25}/P_{24}) \times \ln(P_{25}/P_{24}))}$ | [26] |
| *Compressor 2* | $Z_{\text{Comp2}} = \frac{(71.1 \times \dot{m}_{26})}{(0.9 - \eta_{\text{Compressor}}) \times ((P_{27}/P_{26}) \times \ln(P_{27}/P_{26}))}$ | [26] |
| *Gas turbine* | $Z_{\text{Gas,Turbin}} = \frac{(1536 \times \dot{m}_{32})}{(0.92 - \eta_{\text{Gas,Turbin}}) \times \ln(P_{33}/P_{34}) \times (1 + \exp(0.036 \times T_{33} - 54.4)}$ | [26] |
| *Compressed air energy storage* | $Z_{\text{CAES tank}} = \left(\left(1.218 \times \exp\left(2.3631 + 1.3673 \times \left(\ln\left(V_{\text{Storage}}\right)\right) - 0.06309 \times \left(\ln\left(V_{\text{Storage}}\right)\right)^2\right)\right)\right)$ | [26] |
| *Absorption chiller* | $Z_{\text{Chiller}} = 1144.3 \times \left(Q_{\text{Cooling}}{}^{0.67}\right)$ | [37] |

## Appendix 4

*Appendix 4. The results obtained from the optimal values of the objective functions*

| Number | Geothermal mass flow rate (kg/s) | T1 ($^0$C) | T4 ($^0$C) | T6 ($^0$C) | T8 ($^0$C) | Pinch point evaporator ($^0$C) | ORC turbine efficiency (%) | Pump efficiency (%) | Compressor efficiency (%) | Gas turbine efficiency (%) | P28 (kPa) | ERTE (%) | Cost rate ($/h) | Desirability (%) |
|---|---|---|---|---|---|---|---|---|---|---|---|---|---|---|
| 1 | 3.029 | 206.689 | 152.999 | 66.771 | 65.49 | 5.984 | 0.89 | 0.803 | 0.888 | 0.894 | 4779.956 | 77.981 | 5.489 | 0.955 |
| 2 | 3.029 | 209.222 | 155.298 | 66.819 | 65.431 | 7.207 | 0.893 | 0.756 | 0.891 | 0.894 | 4771.973 | 77.701 | 5.496 | 0.95 |
| 3 | 3.286 | 207.696 | 155.491 | 66.764 | 65.491 | 5.994 | 0.894 | 0.808 | 0.881 | 0.868 | 5192.721 | 77.441 | 5.556 | 0.944 |
| 4 | 3.029 | 208.775 | 155.121 | 66.918 | 65.491 | 5.902 | 0.868 | 0.782 | 0.894 | 0.886 | 5209.826 | 77.307 | 5.357 | 0.943 |
| 5 | 3.166 | 204.657 | 151.194 | 66.764 | 65.315 | 6.69 | 0.894 | 0.851 | 0.89 | 0.894 | 4725.458 | 77.127 | 5.483 | 0.939 |
| 6 | 3.029 | 211.393 | 155.462 | 66.78 | 65.491 | 6.969 | 0.892 | 0.782 | 0.894 | 0.834 | 5122.144 | 76.968 | 5.489 | 0.936 |
| 7 | 3.029 | 210.227 | 155.347 | 66.818 | 65.491 | 6.702 | 0.892 | 0.822 | 0.87 | 0.844 | 5091.616 | 76.761 | 5.489 | 0.932 |
| 8 | 3.029 | 209.371 | 154.393 | 66.77 | 65.491 | 5.902 | 0.882 | 0.756 | 0.886 | 0.86 | 5257.235 | 77.391 | 6.216 | 0.932 |
| 9 | 3.029 | 203.652 | 149.216 | 66.764 | 65.491 | 6.624 | 0.894 | 0.803 | 0.867 | 0.894 | 5021.341 | 76.686 | 5.489 | 0.931 |
| 10 | 3.369 | 205.432 | 155.417 | 66.767 | 65.34 | 5.902 | 0.882 | 0.841 | 0.869 | 0.894 | 4725.753 | 76.648 | 5.489 | 0.93 |
| 11 | 3.037 | 206.927 | 152.396 | 66.764 | 65.491 | 6.123 | 0.893 | 0.849 | 0.855 | 0.894 | 5166.418 | 77.736 | 6.767 | 0.929 |
| 12 | 3.037 | 201.761 | 147.366 | 66.777 | 65.32 | 5.91 | 0.894 | 0.864 | 0.894 | 0.861 | 5182.243 | 76.437 | 5.489 | 0.926 |
| 13 | 3.034 | 202.823 | 149.363 | 67.919 | 65.49 | 5.902 | 0.892 | 0.762 | 0.894 | 0.884 | 5274.33 | 76.419 | 5.48 | 0.926 |
| 14 | 3.029 | 210.611 | 155.491 | 66.764 | 65.49 | 5.902 | 0.894 | 0.843 | 0.868 | 0.816 | 4857.553 | 76.8 | 6.054 | 0.924 |
| 15 | 3.029 | 212.945 | 155.485 | 66.764 | 65.491 | 6.597 | 0.853 | 0.798 | 0.894 | 0.891 | 4806.275 | 77.647 | 7.128 | 0.921 |
| 16 | 3.029 | 202.74 | 150.248 | 66.764 | 65.491 | 6.518 | 0.892 | 0.865 | 0.853 | 0.894 | 5270.128 | 76.146 | 5.493 | 0.921 |
| 17 | 3.032 | 210.424 | 155.491 | 67.423 | 65.491 | 6.606 | 0.894 | 0.873 | 0.886 | 0.816 | 4728.017 | 76.109 | 5.489 | 0.92 |
| 18 | 3.39 | 206.726 | 155.487 | 66.764 | 64.367 | 7.136 | 0.894 | 0.834 | 0.891 | 0.875 | 5274.483 | 76.067 | 5.489 | 0.919 |
| 19 | 3.202 | 201.418 | 149.145 | 66.763 | 65.491 | 6.368 | 0.894 | 0.793 | 0.86 | 0.894 | 4821.663 | 75.992 | 5.183 | 0.918 |
| 20 | 3.029 | 209.703 | 154.017 | 66.763 | 65.487 | 7.543 | 0.855 | 0.814 | 0.886 | 0.894 | 5091.545 | 75.915 | 5.484 | 0.917 |
| 21 | 3.34 | 210.948 | 155.491 | 66.764 | 65.424 | 7.674 | 0.893 | 0.781 | 0.894 | 0.864 | 5163.996 | 77.184 | 6.908 | 0.917 |
| 22 | 3.029 | 205.204 | 155.08 | 66.767 | 65.491 | 6.652 | 0.894 | 0.836 | 0.826 | 0.894 | 5051.376 | 75.784 | 5.26 | 0.914 |
| 23 | 3.317 | 202.237 | 147.721 | 66.763 | 65.49 | 7.231 | 0.894 | 0.839 | 0.894 | 0.87 | 4861.824 | 75.686 | 5.489 | 0.912 |
| 24 | 3.032 | 206.216 | 148.553 | 66.765 | 65.491 | 7.49 | 0.894 | 0.756 | 0.894 | 0.88 | 4876.47 | 76.755 | 6.875 | 0.909 |
| 25 | 3.075 | 205.713 | 153.785 | 67.345 | 65.491 | 7.131 | 0.894 | 0.818 | 0.834 | 0.894 | 4898.313 | 75.531 | 5.489 | 0.909 |
| 26 | 3.029 | 213.233 | 155.49 | 66.815 | 65.473 | 7.02 | 0.894 | 0.868 | 0.85 | 0.884 | 5181.058 | 78.647 | 8.845 | 0.908 |
| 27 | 3.029 | 211.063 | 155.491 | 68.138 | 65.183 | 7.417 | 0.873 | 0.771 | 0.894 | 0.859 | 4950.509 | 75.428 | 5.489 | 0.907 |
| 28 | 3.113 | 203.733 | 147.297 | 66.798 | 65.491 | 6.637 | 0.894 | 0.779 | 0.894 | 0.832 | 5019.879 | 75.418 | 5.489 | 0.907 |
| 29 | 3.035 | 209.967 | 155.491 | 66.807 | 65.046 | 5.902 | 0.829 | 0.8 | 0.88 | 0.893 | 4909.143 | 75.604 | 5.775 | 0.906 |
| 30 | 3.029 | 207.513 | 155.491 | 67.224 | 63.203 | 6.418 | 0.857 | 0.894 | 0.894 | 0.894 | 5030.081 | 75.239 | 5.39 | 0.904 |
| 31 | 3.034 | 209.103 | 152.127 | 66.77 | 64.684 | 6.993 | 0.843 | 0.86 | 0.89 | 0.872 | 4940.586 | 74.941 | 5.697 | 0.895 |
| 32 | 3.029 | 209.011 | 152.149 | 66.764 | 65.491 | 6.057 | 0.894 | 0.771 | 0.871 | 0.767 | 4959.369 | 74.717 | 5.489 | 0.894 |
| 33 | 3.029 | 198.907 | 145.837 | 66.764 | 65.488 | 6.379 | 0.894 | 0.869 | 0.865 | 0.841 | 5274.541 | 74.434 | 4.952 | 0.888 |
| 34 | 3.252 | 204.298 | 155.491 | 66.764 | 61.68 | 7.502 | 0.894 | 0.891 | 0.894 | 0.893 | 4795.814 | 74.363 | 5.779 | 0.882 |
| 35 | 3.202 | 199.202 | 144.509 | 66.764 | 65.451 | 6.879 | 0.851 | 0.813 | 0.893 | 0.894 | 5087.708 | 74.12 | 5.453 | 0.882 |
| 36 | 3.029 | 209.011 | 149.532 | 66.764 | 65.491 | 7.289 | 0.871 | 0.855 | 0.894 | 0.818 | 4733.388 | 74.856 | 6.445 | 0.881 |
| 37 | 3.029 | 202.343 | 147.201 | 66.792 | 65.478 | 5.902 | 0.873 | 0.756 | 0.844 | 0.866 | 5253.074 | 74.843 | 6.51 | 0.88 |
| 38 | 3.029 | 196.85 | 144.513 | 66.765 | 64.096 | 7.109 | 0.875 | 0.894 | 0.893 | 0.894 | 4725.464 | 73.964 | 5.21 | 0.879 |
| 39 | 3.047 | 210.236 | 152.114 | 66.763 | 65.037 | 6.078 | 0.83 | 0.84 | 0.894 | 0.817 | 4976.797 | 73.875 | 5.489 | 0.877 |
| 40 | 3.034 | 211.706 | 151.439 | 66.764 | 65.488 | 7.175 | 0.894 | 0.89 | 0.894 | 0.758 | 4859.44 | 74.939 | 6.846 | 0.876 |
| 41 | 3.029 | 213.236 | 152.664 | 67.724 | 65.486 | 7.197 | 0.869 | 0.864 | 0.846 | 0.894 | 5099.567 | 77.061 | 9.116 | 0.876 |
| 42 | 3.029 | 212.69 | 154.969 | 66.764 | 65.491 | 5.985 | 0.89 | 0.807 | 0.805 | 0.82 | 5152.493 | 76.36 | 8.489 | 0.875 |
| 43 | 3.029 | 211.548 | 155.411 | 67.507 | 63.538 | 6.881 | 0.839 | 0.894 | 0.894 | 0.891 | 4747.13 | 75.324 | 7.403 | 0.874 |
| 44 | 4.511 | 205.359 | 155.488 | 66.764 | 65.442 | 5.902 | 0.894 | 0.76 | 0.894 | 0.761 | 5044.398 | 73.379 | 5.489 | 0.867 |
| 45 | 3.029 | 213.166 | 149.394 | 66.764 | 65.491 | 7.404 | 0.894 | 0.826 | 0.882 | 0.83 | 5258.452 | 77.253 | 9.867 | 0.866 |
| 46 | 3.113 | 213.237 | 150.998 | 66.763 | 65.491 | 6.856 | 0.894 | 0.871 | 0.783 | 0.878 | 5058.57 | 77.562 | 10.431 | 0.861 |
| 47 | 3.838 | 200.093 | 153.782 | 69.597 | 65.298 | 5.902 | 0.889 | 0.788 | 0.843 | 0.894 | 4725.63 | 73.053 | 5.489 | 0.861 |
| 48 | 3.068 | 209.642 | 155.491 | 71.193 | 65.475 | 6.753 | 0.891 | 0.894 | 0.874 | 0.795 | 4875.652 | 72.897 | 5.51 | 0.857 |

(*continued on next page*)

(*continued*)

| Number | Geothermal mass flow rate (kg/s) | T1 ($^0$C) | T4 ($^0$C) | T6 ($^0$C) | T8 ($^0$C) | Pinch point evaporator ($^0$C) | ORC turbine efficiency (%) | Pump efficiency (%) | Compressor efficiency (%) | Gas turbine efficiency (%) | P28 (kPa) | ERTE (%) | Cost rate ($/h) | Desirability (%) |
|---|---|---|---|---|---|---|---|---|---|---|---|---|---|---|
| 49 | 3.029 | 208.702 | 149.65 | 66.764 | 65.491 | 6.575 | 0.894 | 0.799 | 0.812 | 0.784 | 4778.308 | 74.073 | 7.076 | 0.856 |
| 50 | 3.049 | 205.968 | 150.007 | 66.763 | 65.481 | 7.738 | 0.894 | 0.882 | 0.788 | 0.893 | 5067.804 | 75.195 | 8.393 | 0.856 |
| 51 | 3.906 | 198.757 | 147.843 | 66.834 | 65.484 | 8.098 | 0.87 | 0.778 | 0.894 | 0.87 | 5268.416 | 72.548 | 5.125 | 0.851 |
| 52 | 3.029 | 198.561 | 144.509 | 67.827 | 65.318 | 6.155 | 0.824 | 0.757 | 0.891 | 0.891 | 5273.833 | 72.415 | 5.489 | 0.848 |
| 53 | 3.029 | 213.005 | 147.117 | 66.764 | 65.199 | 6.1 | 0.893 | 0.76 | 0.758 | 0.856 | 5082.374 | 76.612 | 10.288 | 0.848 |
| 54 | 3.029 | 199.288 | 146.167 | 66.765 | 62.253 | 5.902 | 0.894 | 0.821 | 0.89 | 0.788 | 4737.408 | 72.338 | 5.489 | 0.846 |
| 55 | 3.387 | 205.291 | 149.25 | 66.763 | 65.49 | 8.098 | 0.891 | 0.834 | 0.87 | 0.774 | 5111.638 | 72.465 | 5.712 | 0.846 |
| 56 | 3.03 | 202.208 | 144.587 | 68.835 | 65.491 | 5.902 | 0.894 | 0.858 | 0.824 | 0.839 | 5180.916 | 74.073 | 7.766 | 0.845 |
| 57 | 3.029 | 211.042 | 145.369 | 66.764 | 65.491 | 6.31 | 0.893 | 0.893 | 0.781 | 0.843 | 5096.616 | 76.375 | 10.224 | 0.845 |
| 58 | 3.043 | 213.236 | 155.059 | 66.763 | 65.491 | 8.005 | 0.789 | 0.894 | 0.887 | 0.861 | 4789.683 | 72.543 | 6.071 | 0.842 |
| 59 | 3.029 | 213.236 | 151.938 | 66.779 | 65.49 | 7.5 | 0.893 | 0.893 | 0.796 | 0.778 | 5103.344 | 74.386 | 8.373 | 0.841 |
| 60 | 3.031 | 208.589 | 151.224 | 66.764 | 65.491 | 6.898 | 0.832 | 0.757 | 0.847 | 0.811 | 4741.307 | 71.914 | 5.489 | 0.838 |
| 61 | 3.428 | 200.698 | 147.413 | 66.763 | 63.801 | 6.53 | 0.81 | 0.756 | 0.894 | 0.894 | 5071.526 | 71.701 | 5.481 | 0.833 |
| 62 | 4.221 | 206.493 | 153.634 | 66.773 | 65.487 | 6.818 | 0.851 | 0.891 | 0.891 | 0.764 | 5274.55 | 71.683 | 5.489 | 0.833 |
| 63 | 3.029 | 213.236 | 146.79 | 66.764 | 62.666 | 6.696 | 0.89 | 0.811 | 0.758 | 0.854 | 4952.238 | 75.105 | 9.783 | 0.83 |
| 64 | 3.029 | 212.175 | 155.491 | 72.147 | 64.386 | 7.068 | 0.894 | 0.775 | 0.856 | 0.835 | 5274.499 | 73.422 | 7.987 | 0.829 |
| 65 | 3.029 | 201.859 | 144.509 | 66.965 | 65.491 | 6.016 | 0.857 | 0.885 | 0.877 | 0.758 | 4823.845 | 71.638 | 5.701 | 0.829 |
| 66 | 3.119 | 196.811 | 144.516 | 66.764 | 65.474 | 6.158 | 0.88 | 0.791 | 0.81 | 0.796 | 4850.463 | 71.333 | 5.489 | 0.826 |
| 67 | 4.449 | 211.04 | 155.481 | 66.765 | 63.249 | 6.231 | 0.894 | 0.778 | 0.894 | 0.8 | 5101.122 | 75.622 | 10.67 | 0.824 |
| 68 | 3.029 | 197.104 | 146.494 | 66.764 | 65.491 | 7.45 | 0.894 | 0.811 | 0.873 | 0.782 | 4945.351 | 71.123 | 1.955 | 0.821 |
| 69 | 3.029 | 213.223 | 148.608 | 66.764 | 62.559 | 5.905 | 0.894 | 0.851 | 0.756 | 0.789 | 5049.64 | 74.066 | 9.507 | 0.816 |
| 70 | 3.08 | 213.236 | 152.764 | 66.768 | 65.477 | 5.927 | 0.851 | 0.894 | 0.804 | 0.761 | 4731.756 | 73.088 | 8.406 | 0.816 |
| 71 | 4.039 | 212.989 | 155.489 | 68.71 | 65.491 | 7.975 | 0.865 | 0.769 | 0.892 | 0.894 | 5274.55 | 76.102 | 11.572 | 0.816 |
| 72 | 3.029 | 213.236 | 148.122 | 69.744 | 65.491 | 6.886 | 0.894 | 0.893 | 0.756 | 0.794 | 4899.768 | 73.122 | 8.602 | 0.814 |
| 73 | 3.041 | 213.237 | 150.201 | 68.418 | 64.62 | 7.954 | 0.84 | 0.756 | 0.851 | 0.894 | 5134.71 | 74.152 | 10.066 | 0.809 |
| 74 | 3.029 | 206.152 | 144.749 | 70.368 | 65.491 | 7.06 | 0.894 | 0.782 | 0.756 | 0.89 | 5226.069 | 73.476 | 9.353 | 0.808 |
| 75 | 3.031 | 196.764 | 148.457 | 70.017 | 65.329 | 6.132 | 0.863 | 0.893 | 0.823 | 0.866 | 5115.873 | 70.463 | 3.717 | 0.807 |
| 76 | 3.083 | 213.208 | 151.855 | 66.765 | 60.024 | 6.471 | 0.894 | 0.821 | 0.847 | 0.771 | 5129.282 | 73.432 | 9.434 | 0.806 |
| 77 | 5.386 | 199.539 | 154.889 | 66.771 | 65.491 | 7.867 | 0.878 | 0.893 | 0.859 | 0.82 | 5274.541 | 70.245 | 5.489 | 0.802 |
| 78 | 5.914 | 197.668 | 155.491 | 67.302 | 65.386 | 7.22 | 0.891 | 0.866 | 0.852 | 0.83 | 4807.977 | 70.282 | 5.609 | 0.802 |
| 79 | 3.029 | 201.093 | 149.427 | 66.936 | 65.491 | 6.636 | 0.892 | 0.881 | 0.767 | 0.78 | 5274.55 | 71.05 | 6.933 | 0.799 |
| 80 | 3.029 | 206.376 | 149.644 | 66.763 | 64.284 | 8.006 | 0.893 | 0.856 | 0.797 | 0.766 | 4725.495 | 71.223 | 7.421 | 0.795 |
| 81 | 3.029 | 208.921 | 149.088 | 66.852 | 65.41 | 6.125 | 0.778 | 0.894 | 0.879 | 0.773 | 5146.733 | 69.736 | 5.479 | 0.791 |
| 82 | 3.915 | 207.75 | 155.423 | 66.799 | 65.183 | 5.992 | 0.81 | 0.811 | 0.854 | 0.757 | 4887.228 | 69.579 | 5.489 | 0.788 |
| 83 | 3.029 | 209.05 | 145.769 | 71.76 | 65.203 | 8.087 | 0.894 | 0.756 | 0.756 | 0.894 | 4739.909 | 72.506 | 9.96 | 0.78 |
| 84 | 4.034 | 206.737 | 147.212 | 66.764 | 64.988 | 5.902 | 0.884 | 0.756 | 0.756 | 0.835 | 5263.786 | 74.142 | 11.737 | 0.78 |
| 85 | 3.118 | 205.172 | 152.367 | 69.066 | 58.597 | 6.08 | 0.894 | 0.894 | 0.894 | 0.792 | 4725.712 | 70.936 | 8.084 | 0.779 |
| 86 | 3.46 | 208.696 | 145.079 | 66.764 | 65.484 | 8.074 | 0.894 | 0.772 | 0.772 | 0.777 | 4731.428 | 72.36 | 9.968 | 0.777 |
| 87 | 5.941 | 202.123 | 155.481 | 66.764 | 65.491 | 8.098 | 0.825 | 0.756 | 0.881 | 0.876 | 4793.497 | 70.076 | 7.218 | 0.774 |
| 88 | 3.565 | 213.033 | 144.509 | 66.763 | 64.37 | 8.098 | 0.883 | 0.841 | 0.756 | 0.802 | 4725.505 | 72.914 | 10.989 | 0.771 |
| 89 | 3.041 | 196.764 | 144.509 | 66.763 | 60.789 | 7 | 0.891 | 0.859 | 0.776 | 0.892 | 4804.785 | 71.48 | 9.614 | 0.766 |

(*continued on next page*)

(*continued*)

| Number | Geothermal mass flow rate (kg/s) | T1 ($^0$C) | T4 ($^0$C) | T6 ($^0$C) | T8 ($^0$C) | Pinch point evaporator ($^0$C) | ORC turbine efficiency (%) | Pump efficiency (%) | Compressor efficiency (%) | Gas turbine efficiency (%) | P28 (kPa) | ERTE (%) | Cost rate ($/h) | Desirability (%) |
|---|---|---|---|---|---|---|---|---|---|---|---|---|---|---|
| 90 | 3.03 | 213.236 | 152.043 | 75.942 | 65.491 | 7.728 | 0.894 | 0.894 | 0.766 | 0.843 | 5096.274 | 70.748 | 8.762 | 0.765 |
| 91 | 5.874 | 205.232 | 155.315 | 72.336 | 65.491 | 5.902 | 0.894 | 0.812 | 0.894 | 0.757 | 5038.043 | 70.647 | 9.698 | 0.749 |
| 92 | 3.029 | 213.236 | 144.985 | 66.764 | 59.054 | 5.902 | 0.816 | 0.759 | 0.849 | 0.885 | 5272.28 | 72.488 | 12.005 | 0.746 |
| 93 | 7.75 | 196.792 | 151.556 | 66.764 | 65.478 | 8.067 | 0.878 | 0.757 | 0.893 | 0.798 | 4978.627 | 69.325 | 8.214 | 0.744 |
| 94 | 3.029 | 212.973 | 144.51 | 66.886 | 58.924 | 6.739 | 0.84 | 0.846 | 0.756 | 0.756 | 5104.314 | 68.388 | 7.111 | 0.739 |
| 95 | 3.029 | 208.888 | 144.509 | 71.069 | 65.491 | 7.548 | 0.852 | 0.81 | 0.756 | 0.756 | 4894.623 | 68.053 | 7.137 | 0.731 |
| 96 | 3.691 | 206.224 | 155.491 | 66.816 | 58.017 | 5.902 | 0.81 | 0.79 | 0.874 | 0.886 | 5274.514 | 70.276 | 10.562 | 0.728 |
| 97 | 3.029 | 213.236 | 152.233 | 67.465 | 64.513 | 8.086 | 0.779 | 0.87 | 0.788 | 0.806 | 4725.462 | 68.314 | 7.838 | 0.728 |
| 98 | 4.941 | 207.395 | 155.491 | 69.078 | 64.982 | 6.682 | 0.846 | 0.894 | 0.778 | 0.894 | 4731.98 | 72.196 | 13.042 | 0.723 |
| 99 | 5.611 | 198.39 | 155.285 | 66.764 | 65.484 | 8.098 | 0.84 | 0.894 | 0.821 | 0.781 | 4842.536 | 66.162 | 5.489 | 0.709 |
| 100 | 5.779 | 203.049 | 155.483 | 73.564 | 65.491 | 8.067 | 0.889 | 0.813 | 0.889 | 0.761 | 5273.814 | 67.298 | 7.94 | 0.704 |

## Data availability

Data will be made available on request.

## References


[1] T. Akan, Renewable energy: moderated, moderating or mediating? Appl. Energy 347 (2023) 121411.
[2] S. Morimoto, et al., Scenario assessment of introducing carbon utilization and carbon removal technologies considering future technological transition based on renewable energy and direct air capture, J. Clean. Prod. 402 (2023) 136763.
[3] B.M.S. Giambastiani, et al., Energy performance strategies for the large scale introduction of geothermal energy in residential and industrial buildings: the GEO. POWER project, Energy Pol. 65 (2014) 315–322.
[4] G. Axelsson, 7.01 - introduction to volume on geothermal energy, in: second ed., in: T.M. Letcher (Ed.), Comprehensive Renewable Energy, Elsevier, Oxford, 2022, pp. 1–2.
[5] M. Adib, et al., Integrating wind energy and compressed air energy storage for remote communities: a bi-level programming approach, J. Energy Storage 72 (2023) 108496.
[6] X. Liu, et al., The investigation on a hot dry rock compressed air energy storage system, Energy Convers. Manag. 291 (2023) 117274.
[7] A.R. Razmi, M. Soltani, A. Ardehali, K. Gharali, M.B. Dusseault, J. Nathwani, Design, thermodynamic, and wind assessments of a compressed air energy storage (CAES) integrated with two adjacent wind farms: a case study at Abhar and Kahak sites, Iran, Energy 221 (2021) 119902.
[8] A.R. Razmi, M. Soltani, M. Torabi, Investigation of an efficient and environmentally-friendly CCHP system based on CAES, ORC and compression-absorption refrigeration cycle: energy and exergy analysis, Energy Convers. Manag. 195 (2019) 1199–1211.
[9] A.R. Razmi, M. Janbaz, Exergoeconomic assessment with reliability consideration of a green cogeneration system based on compressed air energy storage (CAES), Energy Convers. Manag. 204 (October) (2020) 112320.
[10] S.M. Alirahmi, A.R. Razmi, A. Arabkoohsar, Comprehensive assessment and multi-objective optimization of a green concept based on a combination of hydrogen and compressed air energy storage (CAES) systems, Renew. Sustain. Energy Rev. 142 (2021) 110850.
[11] S.M. Alirahmi, S.F. Mousavi, P. Ahmadi, A. Arabkoohsar, Soft computing analysis of a compressed air energy storage and SOFC system via different artificial neural network architecture and tri-objective grey wolf optimization, Energy 236 (2021) 121412.
[12] M. Seiiedhoseiny, et al., Exergoeconomic analysis and optimization of a high-efficient multi-generation system powered by Sabalan (Savalan) geothermal power plant including branched GAX cycle and electrolyzer unit, Energy Convers. Manag. 268 (2022) 115996.
[13] J. Pan, et al., Energy, exergy and economic analysis of different integrated systems for power generation using LNG cold energy and geothermal energy, Renew. Energy 202 (2023) 1054–1070.
[14] W. Jiansheng, et al., Numerical investigation on power generation performance of enhanced geothermal system with horizontal well, Appl. Energy 325 (2022) 119865.
[15] H. Li, F. Liang, P. Guo, C. He, S. Li, S. Zhou, L. Deng, C. Bai, X. Zhang, G. Zhang, Study on the biomass-based SOFC and ground source heat pump coupling cogeneration system, Appl. Therm. Eng. 165 (2020) 114527.
[16] K.H.M. Al-Hamed, I. Dincer, Investigation of a concentrated solar-geothermal integrated system with a combined ejector-absorption refrigeration cycle for a small community, Int. J. Refrig. 106 (2019) 407–426.
[17] S. Briolaa, R. Gabbrielli, A. Bischi, Off-design performance analysis of a novel hybrid binary geothermalbiomasspower plant in extreme environmental conditions, Energy Convers. Manag. 195 (2019) 210–225.
[18] C. Zhong, et al., The feasibility of clean power generation from a novel dual-vertical-well enhanced geothermal system (EGS): a case study in the Gonghe Basin, China, J. Clean. Prod. 344 (2022) 131109.
[19] A.H. Mardan Dezfouli, et al., Energy, exergy, and exergoeconomic analysis and multi-objective optimization of a novel geothermal driven power generation system of combined transcritical CO2 and C5H12 ORCs coupled with LNG stream injection, Energy 262 (2023) 125316.
[20] B. Ghorbani, R. Shirmohammadi, M. Mehrpooya, Development of an innovative cogeneration system for fresh water and power production by renewable energy using thermal energy storage system, Sustain. Energy Technol. Assessments 37 (2020) 100572.
[21] A. Karapekmez, I. Dincer, Comparative efficiency and environmental impact assessments of a solar-assisted combined cycle with various fuels, Appl. Therm. Eng. 114409 (2020).
[22] Hadis Montazerinejad, Ahmadi Pouria, Montazerinejad Zeynab, Advanced exergy, exergo-economic and exrgo-environmental analyses of a solar based trigeneration energy system, Appl. Therm. Eng. 152 (2019) 666–685.
[23] H. Shakibi, et al., Exergoeconomic and optimization study of a solar and wind-driven plant employing machine learning approaches; a case study of Las Vegas city, J. Clean. Prod. 385 (2023) 135529.
[24] E. Assareh, et al., An integrated system for producing electricity and fresh water from a new gas-fired power plant and a concentrated solar power plant – case study – (Australia, Spain, South Korea, Iran), Renew. Energy Focus 44 (2023) 19–39.
[25] E. Assareh, et al., Transient thermodynamic modeling and economic assessment of cogeneration system based on compressed air energy storage and multi-effect desalination, J. Energy Storage 55 (2022) 105683.
[26] D.L. Allaix, V.I. Carbone, An improvement of the response surface method, Struct. Saf. 33 (2) (2011) 165–172.
[27] D.-Q. Li, et al., Response surface methods for slope reliability analysis: review and comparison, Eng. Geol. 203 (2016) 3–14.
[28] M.B. Aryanezhad, M.J. Tarokh, M.N. Mokhtarian, F. Zaheri, A fuzzy TOPSIS method based on left and right scores, Int. J. Ind.Eng.Product. Res. 22 (1) (2011) 51–62.
[29] C.T. Chen, Extensions of TOPSIS for Group Decision–making under fuzzy environment, Fuzzy Set Syst. 114 (2000) 1–9.
[30] A.R. Razmi, Soltani, C.M. Aghanajafi, M. Torabi, Thermodynamic and economic investigation of a novel integration of the absorption-recompression refrigeration system with compressed air energy storage (CAES), Energy Convers. Manag. 187 (2019) 262–273.
[31] E. Assareh, et al., A proposal on a co-generation system accompanied with phase change material to supply energy demand of a hospital to make it a zero energy building (ZEB), Energy Build. 318 (2024) 114478.
[32] A. Bahrami, F. Soltanifar, P. Fallahi, S.S. Meschi, A. Sohani, Energy and economic advantages of using solar stills for renewable energy-based multi-generation of power and hydrogen for residential buildings, Buildings 14 (2024) 1041.
[33] A. Sohani, M. Dehbashi, F. Delfani, S. Hoseinzadeh, Optimal techno-economic and thermo-electrical design for a phase change material enhanced renewable energy driven polygeneration unit using a machine learning assisted lattice Boltzmann method, Eng. Anal. Bound. Elem. 152 (2023) 506–517.
[34] S.M. Alirahmi, S. Bashiri Mousavi, A.R. Razmi, P. Ahmadi, A comprehensive techno-economic analysis and multi-criteria optimization of a compressed air energy storage (CAES) hybridized with solar and desalination units, Energy Convers. Manag. 236 (2021) 114053.
[35] T. Kroegera, F.J. Escobedob, J.H. Hernandezc, S. Varelab, S. Delphinb, J.R.B. Fishera, J. Waldrond, Reforestation as a novel abatement and compliance measure for ground-level ozone 111 (40) (2014).
[36] S. Sedayevatan, A. Bahrami, F. Delfani, A. Sohani, Uncertainty covered techno-enviro-economic viability evaluation of a solar still water desalination unit using Monte Carlo approach, Energies 16 (19) (2023) 6924.
[37] S.M. Alirahmi, E. Assareh, Energy, exergy, and exergoeconomics (3E) analysis and multi-objective optimization of a multigeneration energy system for day and night time power generation-Case study: dezful city, Int. J. Hydrogen Energy 45 (56) (2020) 31555–31573.
[38] S. Bashiri Mousavi, M. Adib, M. Soltani, A.R. Razmi, J. Nathwani, Transient ther- modynamic modeling and economic analysis of an adiabatic compressed air energy storage (A-CAES) based on cascade packed bed thermal energy storage with encapsulated phase change materials, Energy Convers. Manag. 243 (2021) 114379, https://doi.org/10.1016/J.ENCONMAN.2021.114379.

[39] P. Ahmadi, I. Dincer, M.A. Rosen, Exergy, exergoeconomic and environmental analyses and evolutionary algorithm based multi-objective optimization of combined cycle power plants, Energy 36 (10) (2011) 5886–5898.
[40] S.M. Alirahmi, S.F. Mousavi, P. Ahmadi, A. Arabkoohsar, Soft computing analysis of a compressed air energy storage and SOFC system via different artificial neural network architecture and tri-objective grey wolf optimization, Energy 236 (2021) 121412, https://doi.org/10.1016/j.energy.2021.121412.
[41] Y. Cao, H.A. Dhahad, Y.-L. Sun, M. Abdollahi Haghghi, M. Delpisheh, H. Athari, et al., The role of input gas species to the cathode in the oxygen-ion conducting and proton conducting solid oxide fuel cells and their applications: comparative 4E analysis, Int. J. Hydrogen Energy (2021), https://doi.org/10.1016/j.ijhydene.2021.03.111.
[42] A. Dezhdar, et al., A transient model for clean electricity generation using Solar energy and ocean thermal energy conversion (OTEC) - case study: karkheh dam - southwest Iran, Energy Nexus 9 (2023) 100176.
[43] E. Assareh, et al., Thermodynamic-economic optimization of a solar-powered combined energy system with desalination for electricity and freshwater production, Smart Energy 5 (2022) 100062.